

1

Lignin-Derived Materials for Supercapacitors

Jesús Muñiz, Ana K. Cuentas-Gallegos, Miguel Robles, Alfredo Guillén-López, Diego R. Lobato-Peralta, and Jojhar E. Pascoe-Sussoni

Universidad Nacional Autónoma de México, Instituto de Energías Renovables, Priv. Xochicalco s/n, Col. Centro, Temixco, Morelos, CP 62580, México

1.1 Lignocellulosic Biomass Conversion to Value-Added Products

The term lignocellulosic biomass makes reference to organic matter such as dry plants, food, crops, forestry and farming residues, municipal solid wastes, among others [1–3]. At elemental level, its major components are carbon, hydrogen, oxygen, nitrogen, and sulfur, also having traces of metallic species [4]. From the molecular point of view, the principal constituents of lignocellulosic biomass, which are the reason of its name, are cellulose, hemicellulose, and lignin [5].

1.1.1 Cellulose

Cellulose is a compound of the polysaccharide's family and is considered as the most abundant organic polymer in nature [6]. The annual production is higher than 10^{10} tons, reaching up to 1.5×10^{12} tons [7]. The major sources are cotton and wood [8], but it is also usually obtained from other precursors, for example, sugarcane bagasse, orange peels, herbs, corn, wheat, among others [9, 10]. The structure of cellulose is based on anhydroglucan monomers linked by β -1-4 glycosidic linkages, see Figure 1.1 [11, 12]. Cellulose is a fibrous material, biodegradable, resistant, colorless, odorless, and insoluble in water [13]. In Table 1.1 are shown some biomasses and their cellulose content.

Cellulose is usually extracted to obtain value-added products. An easy way to extract it is via solvents. It is well known that cellulose can be dissolved in different substances, being NaOH-based solvents an attractive option because of the low cost and easy recovery [18]. After its extraction, cellulose can be treated to obtain new products for diverse applications:

- *Ethanol production*: Once cellulose is separated from hemicellulose and lignin, it can be subjected to an enzymatic hydrolysis process. Because of this enzymatic

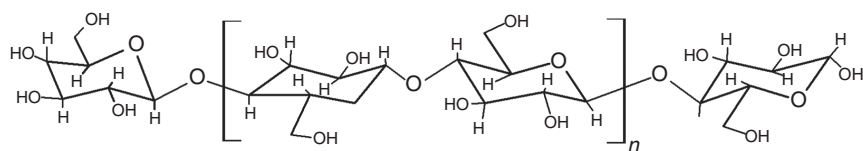


Figure 1.1 Outline of the cellulose molecule.

Table 1.1 Examples of cellulose content in different biomasses.

Biomass	Cellulose content (%)	References
Pine cone	32.7	[14]
Sugarcane	45.8	[15]
Corn grains	27.3	[15]
Coconut shell	40.3	[16]
Peanut shell	42.2	[16]
Sunflower stalk	71.6	[17]
Cotton stalk	66.2	[17]
Oreganum stalk	62.6	[17]

hydrolysis, cellulose is broken down into glucose units, which can be fermented to obtain ethanol.

- **Cellulose fibers:** These materials are characterized by lightweight, low cost, biodegradability, good mechanical properties, among others. Cellulose fibers are often used as a reinforcement material in diverse industries such as automotive, packaging, marine, constructions, and military [19]. Consequently, a variety of precursors such as rice and oat husk can be used [20]. Another important and more recent application for cellulose fibers has been their use as an environmentally friendly binder for battery and supercapacitor (SC) electrodes. This application is making the development of green supercapacitors a reality. Advantages include low price (US\$ 0.5–2 kg⁻¹), large availability, and no chemical processing separation method is required. Additionally, low solubility in a supercapacitor electrolyte and high thermal stability are also available [21–24].
- **Cellulose films/membranes:** Cellulose can be treated to obtain films/membranes with diverse applications such as packaging films, water treatment, and drug wrapping [25–27]. In the field of energy storage, cellulose membranes have been employed as electrode separators in supercapacitors, showing low resistances to charge transfer [28].

1.1.2 Hemicellulose

Hemicellulose is a biopolymer characterized for having a nonlinear structure. After the cellulose, hemicellulose is the most abundant carbohydrate present in the

plant cell walls, representing between 15% and 20% of its mass [29]. The structure of hemicellulose presents branched chains made of units of polysaccharides composed by five or six carbon atoms [30]. These units are galactomannans, such as biopolymers of mannose and galactose, and xyloglucans, e.g. biopolymers of glucose, xylose, and galactose [31] (Figure 1.2). In Table 1.2, some examples of hemicellulose content are presented.

Among the applications of hemicellulose, hydrogels, food additives, emulsifiers, adhesives, adsorbents, and binders in paper making [38, 39] are representative cases. However, although this compound has applications as a binder, it cannot be used in supercapacitor electrodes because these devices usually require liquid electrolytic media, and hemicellulose has soluble portions in an aqueous medium [40].

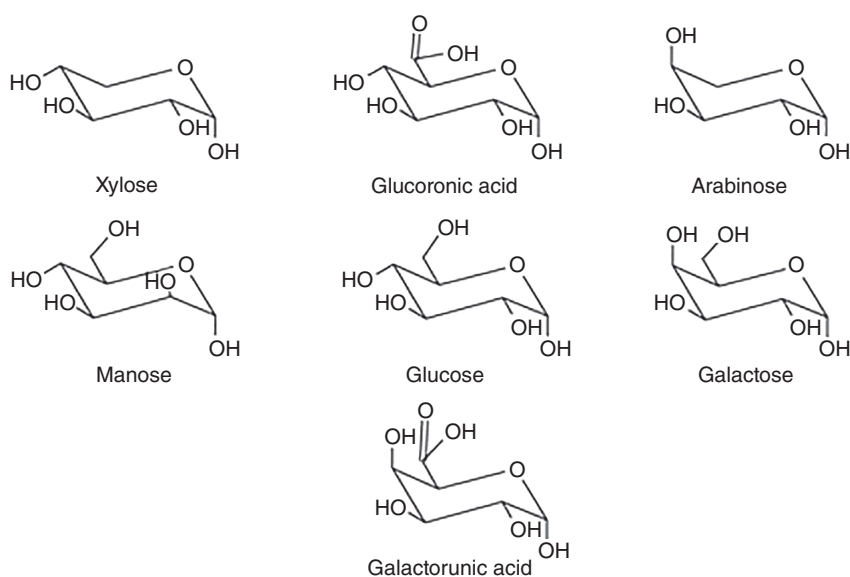


Figure 1.2 Structural units of hemicellulose.

Table 1.2 Examples of hemicellulose content in different biomasses.

Biomass	Hemicellulose content (%)	References
Switchgrass	27.8	[32]
Corn stalk leaf	42.55	[33]
Stone pine	27.0	[34]
Norway spruce	23.1	[34]
Holm oak	30.2	[34]
Grape pomace	7.9	[35]
Wheat straw	36.8	[36]
Bamboo	21.8	[37]

1.1.3 Lignin

Lignin (from the Latin term *lignun*, which means wood [41]) is the name of the most abundant natural phenolic polymer. This compound is formed by a cross-linking structure that contains aliphatic hydroxyl, phenolic hydroxyl, and methoxyl groups and interacts with hemicellulose by ether or ester linkages, being *p*-coumaryl alcohol, coniferyl alcohol, and sinapyl alcohol the principal constituents [42] (Figure 1.3). These precursors are present in high quantities, with a molecular weight between 6×10^5 and 15×10^6 kg kmol⁻¹ [43]. Because of its properties, lignin is the structural component responsible for strength and stiffness of the plant cell walls [44].

There are different classifications for lignin (Figure 1.4). The criterion based on its origin is as follows:

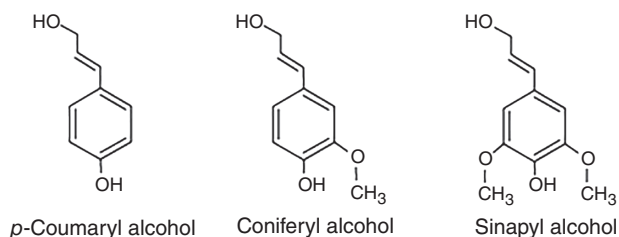


Figure 1.3 Conformational units of lignin.

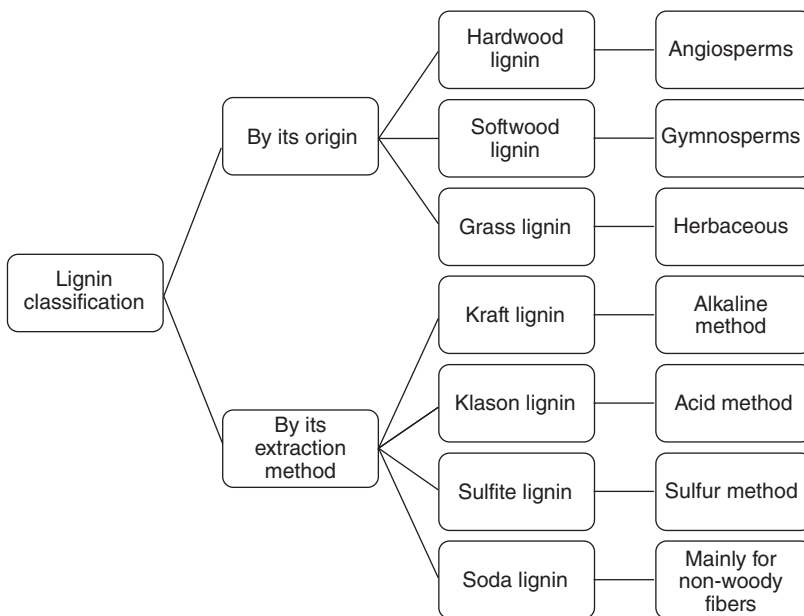


Figure 1.4 Lignin classification by its origin and extraction method.

- *Hardwood lignin*: This term makes reference to lignin from angiosperms, i.e. flowering plants. Angiosperm is the most diverse group in the plant kingdom, including more than 300 000 species [45].
- *Softwood lignin*: This group has its origin in gymnosperms plants, such as pine and spruce [46]. The gymnosperm lineage comprises approximately 1000 species and their main characteristic is that they reproduce by exposed seeds; that is, they do not produce fruit [47].
- *Grass lignin*: This is lignin from herbaceous plants, i.e. nonwoody species [48].

Besides the origin, lignin molecules are also differentiated by their chemical composition. The main components of hardwood lignin are syringyl and guaiacyl, whereas softwood lignin prevails guaiacyl monomers. Finally, in herbaceous lignin, syringyl, guaiacyl, and *p*-hydroxyphenyl are the monomers that prevail [49]. According to the extraction method employed, lignin can be classified in different categories, some of the best known are as follows:

- *Kraft lignin*: The Kraft process to obtain lignin is the most widely used industrially. This process consists in the preparation of a solution, usually called white liquor, based on NaOH and Na₂S solved in water. For this reason, Kraft lignin is also known as alkali lignin. The purpose of white liquor is to produce the fragmentation of lignin molecules into smaller fragments by reacting at temperatures close to 170 °C for about two hours [50]. Kraft process can be divided into three phases [51]. The first one is known as the initial phase (controlled by diffusion). It is a pulping treatment carried out at 150 °C, resulting in dissolution of 20–25% of the lignin present in biomass. The next phase is known as the bulk phase, which occurs in the range of temperatures of 150–170 °C; this phase comprises firstly in an increase of temperature from 150 to 170 °C, followed by a treatment at that temperature (during the bulk phase, the process is controlled by kinetics instead of diffusion). Because of this phase, the dissolution of about 60% of the lignin takes place. The final phase, also known as the residual one, includes a treatment at 170 °C that slowly dissolves 10–15% of lignin present in biomass.
- *Klason lignin*: Contrary to Kraft-type lignin, Klason lignin is obtained by using an acidic solution (72% of H₂SO₄). Klason method consists of acid hydrolysis of extractable-free biomass to separate lignin from cellulose and hemicellulose using the previously acid solution. The biomass is immersed in this solution for two hours at 20 °C under stirring. Then, distilled water at boiling point is added to dilute the solution up to 3%, and a reflux process is performed for four hours to finally recover the lignin by filtration [52, 53].
- *Sulfite lignin*: This is obtained by the sulfite method of preparation of cellulose pulp, which requires the use of calcium, magnesium, ammonium, or sodium sulfite. This process is usual in paper industry to separate lignin from cellulose and hemicellulose. Subsequently, cellulose is isolated. During this process, lignin units undergo the breaking of the C—O bonds that interconnect them. Therefore, the final product is not representative of the original lignin. The process requires digestion of biomass in an aqueous sulfite solution among 140 and 170 °C to perform different chemical reactions. These reactions include breaking in lignin

Table 1.3 Examples of lignin content in different biomasses.

Biomass	Lignin content (%)	References
Sugarcane bagasse	24.39	[59]
Fescue	29.43	[60]
Banana rachis	10.13	[61]
Rice straw	18.00	[62]
Bermuda grass	6.40	[62]
Bamboo	26.00	[62]
Corn cobs	15.78	[62]
Pine straw	22.65	[63]
Wheat straw	20.40	[63]
Flax fiber	14.88	[63]
Olive kernel	33.48	[64]
Peach kernel	47.76	[64]

bonds with carbohydrates, interconnections of lignin units, and the sulfonation of aliphatic lignin chains. To obtain a high-purity material, the product is subjected to a separation process with the purpose to separate hemicellulose and residual carbohydrates through the aforementioned digestion [54].

- *Soda lignin*: Soda methodology is commonly used in the cases of fibers, e.g. sugarcane bagasse [55] and wheat straw [56]. The isolation of soda-type lignin requires the acid precipitation and the patch of different variables. Biomass is mixed with an alkaline solution formed with NaOH in a digester at 170 °C for at least one hour to obtain a liquid, known as black liquor. Later, by filtration, the black liquor is separated from the fibrous material, and sulfuric acid is added to a pH of 3–4. During this step, a noticeable change in coloration is noticed from black to murky brown. Finally, soda lignin is separated from the solution by decanting or vacuum filtered and dried [57, 58].

Some examples of lignin content for different biomasses can be found in Table 1.3.

Lignin is used to be burned in the paper industry as a heat source in the recovery process of chemical agents [65]. On the other hand, in order to produce value-added materials from this precursor, thermochemical processes are the most common route, as described in Section 1.2.

1.2 Production of Carbon Materials by Thermochemical Processes

Thermochemical processes are efficient routes to obtain value-added products from lignocellulosic precursors. The thermochemical processes usually have a greater efficiency because of the amounts of biomass that can be treated and the speed at which

the process occurs [66]. The most common thermochemical conversion routes are hydrothermal liquefaction, gasification, and pyrolysis [67, 68].

1.2.1 Hydrothermal Processing

Hydrothermal processing (HP) is defined as the biomass conversion into biochar, liquid fuels, and gases because of thermal process in a high-pressured water environment, at near- or supercritical conditions, until breaking of the lignocellulosic structure to the aforementioned products. According to the operating conditions, as well as the desired product, hydrothermal processing can be classified as hydrothermal carbonization ($T < 200\text{ }^{\circ}\text{C}$), hydrothermal liquefaction ($200\text{ }^{\circ}\text{C} < T < 375\text{ }^{\circ}\text{C}$), or hydrothermal gasification ($T > 375\text{ }^{\circ}\text{C}$) [69–72].

1.2.1.1 Hydrothermal Processing Mechanism

HP involves many complex reactions. In general, this process requires a pretreatment to reduce particle size, remove contaminants, and can be performed in batch or in continuous. Usually, biomass is processed at $350\text{ }^{\circ}\text{C}$ and 150 bars to generate a phase separation, resulting in CO_2 , biocrude, aqueous phase, and biochar [70]. Despite the occurrence of complex reactions that generate a great variety of products, HP process can be divided into conversion of carbohydrates and conversion of lignin [73, 74].

- *Conversion of carbohydrates:* This makes reference to the reactions that occur in cellulose and hemicellulose caused by the temperature and pressure of the process. Cellulose is soluble in water at subcritical conditions, and it is easily solubilized and hydrolyzed. On the other hand, hemicellulose compared to cellulose is easier to be solubilized and hydrolyzed. It is known that almost 100% of hemicellulose is hydrolyzed after two minutes at $230\text{ }^{\circ}\text{C}$ and 34.5 MPa.
- *Conversion of lignin:* Because of ether bonds present in the lignin structure, during HP, various phenols and methoxy phenols are formed and subsequently degraded to obtain other products. With respect to solid materials (carbon), lignin content in biomass is directly proportional to carbon yield because free phenoxyl radicals formed during HP process reacts to form a solid residue through repolymerization.

Biochars obtained by HP have many applications, for example, generation of metal oxide nanostructures, catalysis, water purification, CO_2 sequestration, and the one that is of interest in this chapter: energy storage [75]. Previous reports indicate that biochars obtained at high pressure conditions in an aqueous environment have properties that make them suitable to be used as electrodes of supercapacitor devices [76, 77].

1.2.2 Gasification

Gasification is defined as the environmentally friendly processing of carbonaceous precursors, such as biomass, coal of mineral origin, among others, into gases, at temperatures among 600 and $1500\text{ }^{\circ}\text{C}$ in a limited oxygen system [78]. The origin of this

process goes back to the 1800s when gas (Town gas) was obtained from coal for lighting and cooking. In the twentieth century, wood gasification gained popularity in Europe for fueling cars [79]. The main products of this process are CO, CO₂, H₂, and CH₄ [80]. The purpose is to obtain a final product with high heating value. The parameters that define the properties of the obtained gasses are related to characteristics of the biomass such as size, density, elemental composition (C, H, O, N, and S), lignocellulosic content, ash content, and moisture content (being a very important parameter, because of biomass with high moisture content, 2260 kJ of extra energy per each kilogram of water is required to react). Additionally, operation parameters and design of the gasification reactor are also important [81].

1.2.2.1 Lignocellulosic Biomass Gasification Mechanism

The gasification process involves various stages as described below [80, 82, 83]:

Drying: In this stage, the biomass moisture is reduced to values of >5% because of the heating effect. This stage occurs in the range of 100–200 °C.

Devolatilization: It is also known as pyrolysis. After drying, thermal treatment of the biomass in a free-oxygen environment takes place at 200–700 °C. During this phase, the biomass is transformed into a solid carbonaceous product, known as biochar, owing to the emission of hydrocarbon gases caused by the decomposition of the precursor into condensable gases that in turn react to become noncondensable (CO, CO₂, H₂, and CH₄).

Oxidation: This stage occurs when the biochar reacts with oxygen at 800–1400 °C, forming carbon monoxide and carbon dioxide (Eqs. (1.1) and (1.2)).

Formation of carbon monoxide ($\Delta H = -111 \text{ kJ mol}^{-1}$):



Formation of carbon dioxide ($\Delta H = -394 \text{ kJ mol}^{-1}$):

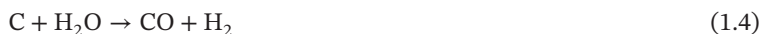


Reduction: It is characterized by the absence of oxygen, and the temperatures in this stage are at 800–1000 °C. The reactions are mainly endothermic, such as Boudouard reaction (Eq. (1.3)) and char gasification (Eq. (1.4)), while water gas shift (Eq. (1.5)) and methanation (Eq. (1.6)) are exothermic.

Boudouard reaction ($\Delta H = 172 \text{ kJ mol}^{-1}$):



Char gasification reaction ($\Delta H = 131.5 \text{ kJ mol}^{-1}$):



Water gas-shift reaction ($\Delta H = -41 \text{ kJ mol}^{-1}$):



Methanation reaction ($\Delta H = -74.8 \text{ kJ mol}^{-1}$):



It is important to remember that in this process, noncondensable gases are the main products. However, a considerable amount of biochar is produced as solid residue [84]. This biochar can be used as a soil biofertilizer when buried, and gasification becomes a process with negative CO₂ balance. That is, a quantity of CO₂ is removed from the atmosphere [85]. Also, by using the biochar obtained as an electrode material in supercapacitive devices, the CO₂ balance of the process becomes neutral.

1.2.3 Pyrolysis

Pyrolysis is the thermal process of biomass in complete absence of oxidizing gas or with a small proportion of it, i.e. secondary oxidation reactions are avoided, inhibiting the production of carbon dioxide. This allows several reactions to be performed, and lignocellulosic components are broken into smaller units. Because of these reactions, different products are obtained (biochar, liquid oil, and gases). It is important to emphasize that the biochar obtained is mainly through to the conversion of lignin because the other lignocellulosic compounds are gasified and transformed into oils because of the increase in temperature [86], with permission of Elsevier.

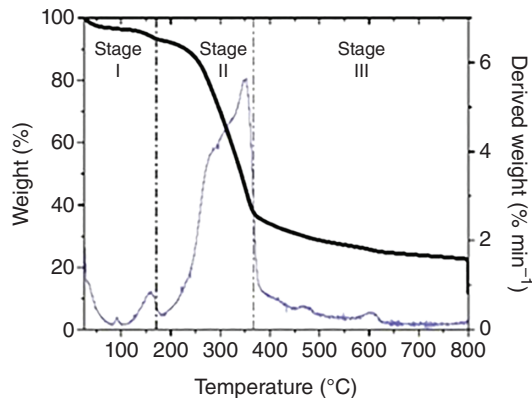
The distribution of these products is based on the process parameters, for example, residence temperature and heating rate [15]. Pyrolysis at temperatures greater than 1000 °C, and long residence times, favors the gas yields. Likewise, temperatures in the range between 500 and 1000 °C and short residence times increase the yield of obtaining oils. Finally, temperatures up to 500 °C benefit the carbon yield [11, 87]. In order to produce biochars with suitable conditions for supercapacitors, temperatures between 600 and 900 °C have proven to be the most appropriate [88–90].

1.2.3.1 Lignocellulosic Biomass Pyrolysis

The pyrolysis process of lignocellulosic biomass does not occur in a single step. Different stages have been studied as a function of resident temperature (Figure 1.5) [88, 91].

Stage I: Dehydration. This stage comprises the temperature range from ambient temperature to 200–220 °C. During this phase, water molecules are separated from the

Figure 1.5 Stages of biomass pyrolysis. Source: Martínez-Casillas et al. [88], with permission of Elsevier.



biomass into steam, without reactions involving the lignocellulosic components [92, 93].

Stage II: Thermal decomposition of lignocellulosic components.

Hemicellulose decomposition: This occurs at temperatures from 200 to 280 °C.

Although the lignocellulosic components do not degrade to a single specific temperature (these processes occur in different ranges). The first component to undergo alterations in its structure due to thermal action is hemicellulose. The hemicellulose molecule begins to decompose at temperatures below 300 °C, predominating at temperatures close to 280 °C.

Cellulose decomposition: This reaction takes place at temperatures 260–350 °C.

Cellulose reacts because of thermal effect to form molecules of anhydrocellulose and levoglucosan. Being cellulose the component present in greater quantity, it is at this stage of the process in which the greatest transformation of biomass occurs [94].

Lignin decomposition: This is the final stage of the process and occurs at temperatures above 280 °C. Subsequent to its thermochemical decomposition, lignin becomes a solid material, rich in carbon (fixed carbon or biochar).

These processes begin at different temperatures, but they occur simultaneously where the temperature ranges are intercepted [93].

Stage III: Formation of stable structures of fixed carbon. Fixed carbon structures are conformed mainly for lignin derivatives.

There are some differences if pyrolysis occurs with the three lignocellulosic components added separately and mixed, in comparison to the original biomass, or individually isolated. Structural decomposition of cellulose, hemicellulose, and lignin occurs at different temperatures because transfer limitations that can be related to heat and/or mass, caused by the mixture, and the effect of inorganic components. Despite that cellulose or hemicellulose is formed of polysaccharides, lignin is formed by heavy cross-linked units of three kinds of benzene–propane, giving it higher thermal stability [95–97]. When pyrolysis is performed at temperatures below 500 °C, the processes that occur in hemicellulose and lignin are exothermic. That is, heat is released mainly because of carbonization. However, at temperatures higher than that, the process becomes endothermic because the main reaction is volatilization [98]. Although there is no clear consensus on the characteristics that define them, pyrolysis is usually classified into three categories according to the parameters of the process (Figure 1.6).

1.2.3.2 Fast Pyrolysis

Fast pyrolysis began in 1973. This process has been used mainly for bio-oil production, with yields of up to 75%. Because of the oil crisis, the prices of this energetic increased very fast, which made it necessary to look for cheaper alternatives. In those years, the first rapid pyrolysis process was based on processing woody biomass at 500 °C [99]. The operational parameters for fast pyrolysis are biomass residence time of about 10–20 seconds [100], high heating ramps, as well as high rates of heat transfer (for which the biomass must be ground), residence times of the vapors generally less than two seconds to minimize secondary reactions, and quick cooling of these

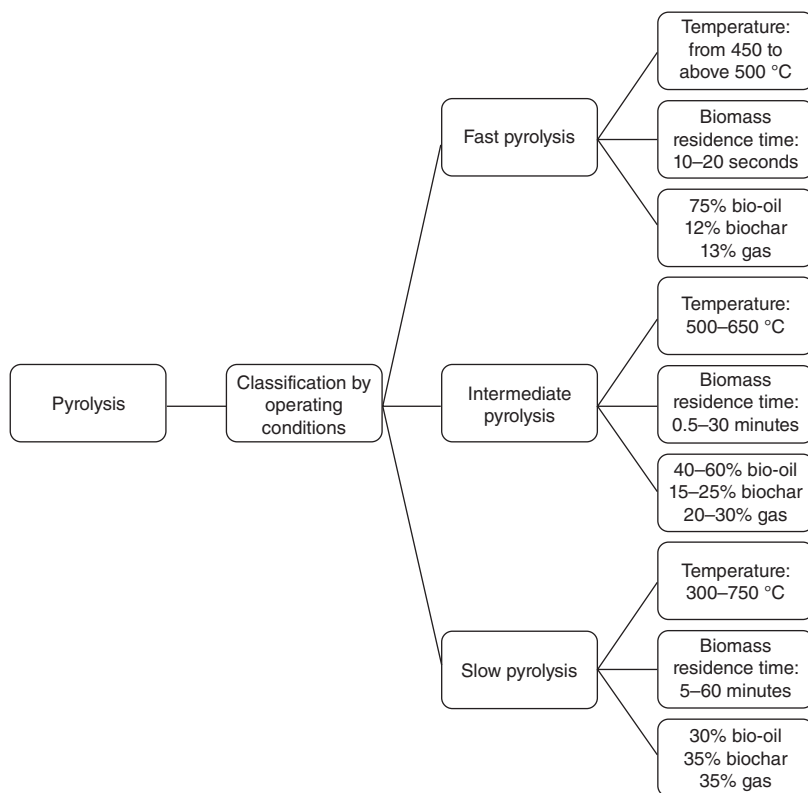


Figure 1.6 Pyrolysis classification.

vapors to obtain the bio-oil as a product [101]. Some authors consider temperatures above 500 °C as the optimal temperature to perform fast pyrolysis for bio-oil production [102]. Others prefer temperatures around 500 °C [101], and there are works in which it was determined to be 450 °C as the most adequate [103].

1.2.3.3 Intermediate Pyrolysis

Intermediate pyrolysis is in the gap between fast and slow pyrolysis. In this category, residence temperature is comprised in the range up to 500 °C and rarely between that of 500–650 °C. In addition, vapor residence time is about 2–4 seconds, and the residence time for the biomass usually is 0.5–30 minutes. Typically, the products are distributed in the range of 40–60% for bio-oil, 20–30% for noncondensable vapors, and 15–25% for biochar [104, 105].

1.2.3.4 Slow Pyrolysis

Slow pyrolysis receives its name because of slower heating ramp, generally about 10 °C min⁻¹ and longer residence times. Some authors consider for slow pyrolysis a residence time between 5 and 30 minutes [100], but others claim that about one hour is correct [106]. Slow pyrolysis is better than fast, and intermediate to obtain biochar due to the obtained yields: 35% for biochar, 30% for bio-oil, and 35% for gas

[107]. Additionally, there is a discrepancy regarding the temperatures that define slow pyrolysis. It is known that this process rises, in most cases, at lower temperatures than $500\text{ }^{\circ}\text{C}$ [102], and other works reject it, arguing that it occurs between 300 and $750\text{ }^{\circ}\text{C}$ [108]. Because this slow pyrolysis is recommended to obtain a greater yield of biochar, this process is more recommended for carbon materials suitable for supercapacitor applications.

1.2.4 Solar Pyrolysis

A sustainable alternative to traditional pyrolysis that uses fossil fuels as a heat source is solar pyrolysis. In this green process, concentrated solar energy is used to replace that provided by nonrenewable sources; thus, this allows to reach a higher energy efficiency in the process. During solar pyrolysis, biomass absorbs energy from the sun to become biofuels in an environmentally friendly process. The main advantage of converting biomass by solar pyrolysis is the sustainability of the process because renewable solar thermal energy is used. Also, higher heating ramps can be reached, as well as higher cooling ramps, because of the volatile compounds, which inhibit secondary reactions [109, 110].

Solar pyrolysis is a viable option because of intensity of solar radiation. It has been determined that the intensity of solar radiation in the Earth's atmosphere corresponds to approximately 1.4 W m^{-2} , while the average over the surface is between 200 and 400 kW m^{-2} for each 24-hour period. However, there are points in latitudes in which up to 1000 kW m^{-2} can be reached [111]. To take advantage of this radiation efficiently, it is necessary to use concentration systems and heliostats (Figure 1.7).

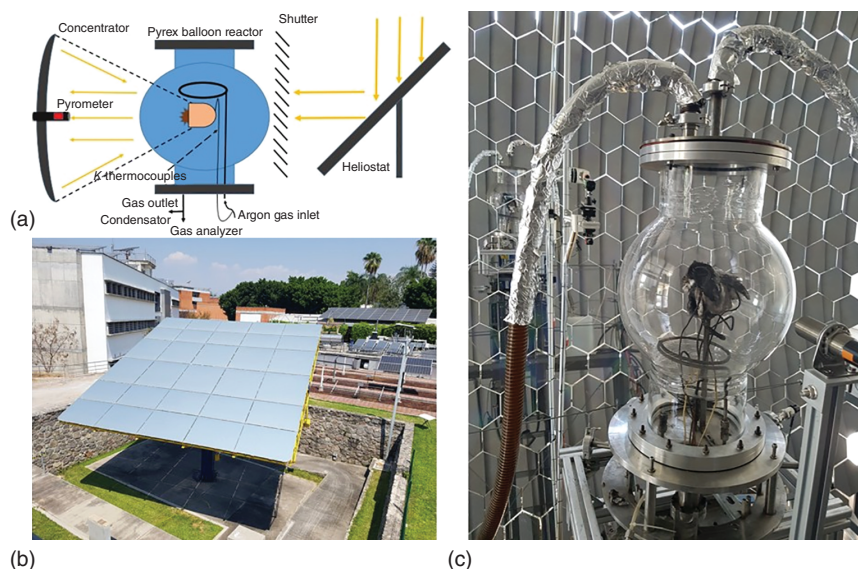


Figure 1.7 Instituto de Energías Renovables-Universidad Nacional Autónoma de México (IER-UNAM) solar furnace HoSIER (by its acronym in Spanish). (a) Schematic diagram. Source: Ayala-Cortés et al. [112], with permission of Elsevier. (b) Heliostat. (c) Concentrator and photoreactor.

In the same way as with traditional pyrolysis, in the solar pyrolysis, the operating conditions have a very important influence on the properties of the obtained products, such as biochar. For example, biochar with properties similar to Vulcan® commercial carbon has been obtained with *Agave angustifolia* as a precursor [112]. Likewise, biochar from pecan nutshell has been the first obtained from solar pyrolysis to be used as a supercapacitor electrode [88].

1.3 Nanoporous Carbon Obtained from Biomass for SC Applications

The term biochar denotes a system formed during the thermochemical conversion of material coming from the biomass found in nature. This may be achieved in a controlled environment of oxygen [113], as it was previously pointed out. Biochar is characterized to be formed in more than 50% of carbon. Typically, this element is present in values between 70% and 80%. Additionally, O, N, H, and S are usually present in smaller quantities, as well as mineral elements such as Na, Mg, K, and Ca [114]. These materials are present in biomass, as discussed above. Because of the intrinsic biomass porosity, biochars usually can have high porosity that yields high surfaces in comparison with other materials depending on the followed thermochemical process. Pores can be classified in four categories according to its size: (i) ultramicropores (width < 1 nm), (ii) micropores (ranging from 1 to 2 nm), (iii) mesopores (ranging from 2 to 50 nm), and (iv) macropores (those pores with sizes larger than 50 nm) [115]. There are routes to increase the porosity of biochar; this process is known as activation. It can be physical or chemical, and it is detailed in Sections 1.3.2, 1.3.2.1, and 1.3.2.2. Porosity of biochar influences various properties, such as the ability to adsorb pollutants [114] and metal particles [116] to improve soil conditions [117]. However, electrochemical applications in supercapacitors are specifically discussed in this chapter.

1.3.1 Supercapacitors

SCs are electric energy storage devices that remain in the gap between conventional capacitors and rechargeable batteries [118]. In Figure 1.8, a visual comparison of such devices, comparing their specific energy and power, is shown. For electric or hybrid vehicles, these devices are the key technologies, and therefore, fuel cells and combustion energy are included for comparison. Nowadays, Li battery technology represents the best energy storage option in the market for electric vehicles, fulfilling the power and energy requirements in combination with price. Nevertheless, there are heat management problems because of their limited power, causing premature degradation of the Li batteries. In general terms, SCs have approximately 100 times more power than a Li battery, and on the order of 10 000 times, the energy of a traditional capacitor [119]. Therefore, SCs can be used in hybrid systems coupled with these battery technologies or separately [120]. It has been previously reported [121] that when an SC is in combination with a Li battery in a hybrid device, the

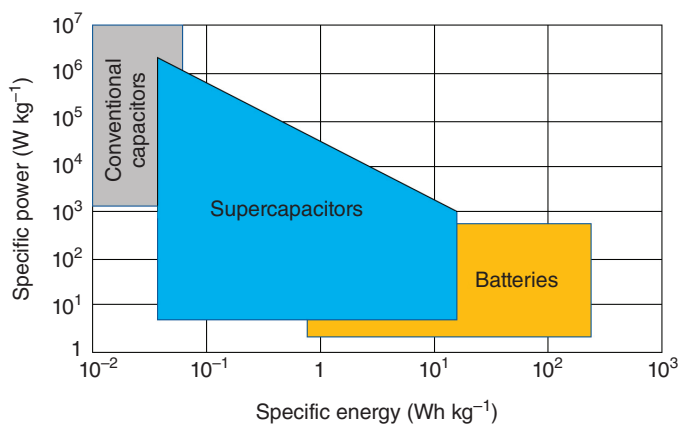


Figure 1.8 Ragone plot of energy storage devices, including fuel cells and combustion energy. Source: Cuentas-Gallegos et al. [118], with permission of Jenny Stanford Publishing.

extra power is provided by the SC, preventing the heat from the battery and therefore protecting it from its degradation. In addition to extending the life of the Li battery, SCs are characterized by a long-life cycle, fast charge–discharge, low maintenance, and cheaper in terms of power [122, 123].

The history of SC goes back to 1957, when the first US patent 2,800,616 by Howard Becker was registered. This patent consisted of capacitor elaborated employing carbon electrodes of great surface [124]. More recently, various materials other than carbon have been tested as supercapacitor electrodes, and it has been determined that they store electrical energy by means of various mechanisms. Furthermore, a classification of supercapacitors has arisen in function of the storage mechanism [125].

1.3.1.1 Electric Double-Layer Capacitors (EDLCs)

Double layer corresponds to the phenomena occurring by charge accumulation in the inter-phase formed when a solid electrode is immersed in an electrolytic medium [118]. The opposite charged ions present in the electrolyte form a layer around the solid electrode to neutralize its electrical charge. The existence of this double layer stores energy analogously to the parallel plates of a conventional capacitor. However, in the SC, the separation between charges is of the order of nanometers instead of centimeters [126, 127]. This mechanism significantly enhances the capacitance properties at the electrode surface. Several theories have emerged to explain the behavior of the double-layer mechanism, which is still a subject of debate.

1. *Helmholtz model*: The first double-layer model was proposed by Helmholtz [128]. His theory established the existence of a compact rigid layer formed by ions around the electrodes of opposite electrical charge at a distance d (Figure 1.9a). The origin of this ion layer is due to the electric potential Ψ_0 of the electrode material. The electric charges stored in this region are responsible for the capacitive behavior of the device. Nowadays, it is known that this model has

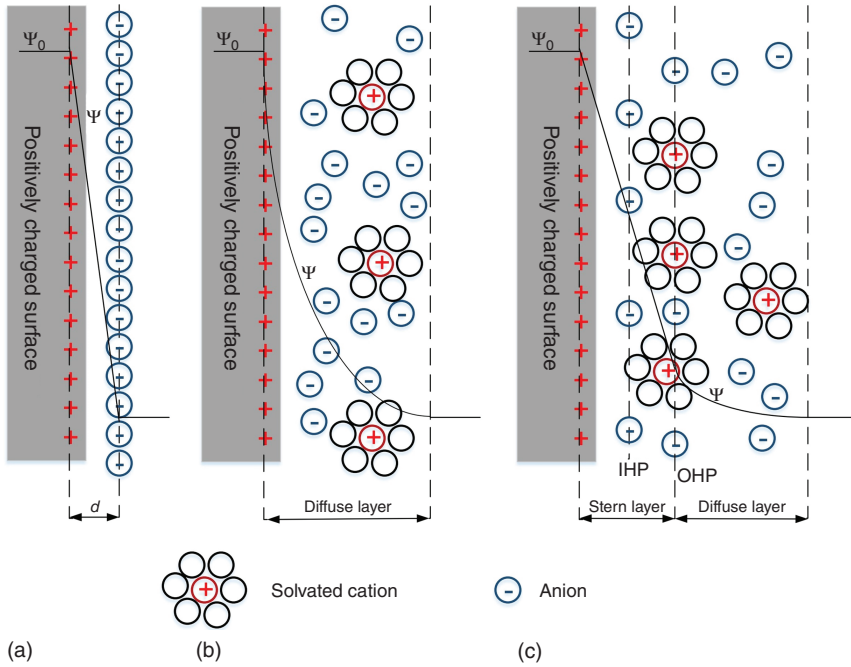


Figure 1.9 Schematic representation of double-layer models. (a) Helmholtz model, (b) Gouy–Chapman model, and (c) Stern model. Source: González et al. [129], with permission of Elsevier.

some deficiencies because it avoids electrostatic interactions beyond the first ion layer and excludes ion concentration in the electrolyte [130]. This model defines the double-layer capacitance as [131]:

$$C = \frac{S_r S_0 A}{d} \quad (1.7)$$

where C = capacitance, S_r = electrolyte dielectric constant, S_0 = dielectric constant of the vacuum, d = charge separation distance, and A = electrode surface area.

2. *Gouy–Chapman model*: This model is established by Louis George Gouy and David Leonard Chapman [132, 133]. Unlike the Helmholtz model, the Gouy–Chapman theory established that the formed layer is not rigid or compact because of the applied potential and electrolyte concentration (Figure 1.9b). Instead of the rigid compact layer, a diffuse layer is formed by the ions solvated in the solution, and it is limited by the counterpotential Ψ . The disadvantage of this model is that it does not explain the behavior of a highly charged double layer [129, 130].
3. *Stern model*: It was proposed by Otto Stern. Stern theory is based on some modifications of the Gouy–Chapman model. This model established the limit of proximity of the ions to the surface of the electrode, suggesting the existence of a compact layer, known as the Stern layer (Figure 1.9c). In this layer, there is a

plane, known as inner Helmholtz plane (IHP), composed by specifically adsorbed ions. Likewise, it was established that the outer Helmholtz plane (OHP) is composed by nonspecifically adsorbed counterions. After the limit of this layer, the diffuse layer is found [134].

1.3.2 Carbon Materials for EDLC

In addition to its large porosity, carbon materials have other properties such as good electric conductivity, low cost, and good electrochemical performance. This is the reason why these materials are the most employed for SC electrodes [118, 135]. Different lignocellulosic precursors have been used to produce biochar with the purpose to be implemented in SC, e.g. pecan nutshell [88], corn straw [136], algae [137], wood [138], flowers [139], and lotus leaf [140]. Nevertheless, it is very important to have in consideration many aspects, such as carbon yield, elemental composition, availability, low price, among others. Likewise, the most appropriate is also to avoid the use of food products [141].

Generally, although not in all cases, carbons that have a greater surface area can store more energy because of the double layer. Some anomalies occur for various reasons, such as electric resistance due to functional groups or defects, pores inaccessible to electrolyte ions, low affinity between the electrode surface and the electrolyte (hydrophilic/hydrophobic behavior), electrolyte decomposition, just to cite some [142]. Therefore, there are processes that help to increase the surface area of the carbon materials through pore opening, known as activation, as detailed below. There are two choices to perform this activation process, namely, chemical and/or physical activation. Each activation methodology involves certain advantages and disadvantages with respect to the other. The chemical route requires lower temperatures than that of the physical route. However, it is usually more expensive, and pollutants are generated by the activating agent. On the other hand, physical activation requires higher temperatures, but it can be more environmentally friendly, with good efficiency. In addition, the pore size distribution (PSD) and surface area obtained by both tracks are usually different [143–146]. Moreover, activated carbons from pecan nutshell have been analyzed as supercapacitor electrodes, reaching up to 150 F g^{-1} of capacitance [88]. On the other hand, carbon from leather waste activated with KOH has reached more than 265 F g^{-1} [147].

1.3.2.1 Physical Activation

Physical activation corresponds to a methodology of two stages that requires agents in gas phase. That is, the presence of CO_2 , steam with or without air, is also necessary. The agents can be used together or separately. However, the separate use of these agents in the same carbon matrix does not produce identical results. The first step of physical activation involves heating the biomass sample under inert atmosphere at temperatures below 1000°C to obtain a biochar by the thermodegradation of its components. The second step is based on heating the biochar at a higher temperature. Nevertheless, instead of using inert atmosphere, an oxidizing agent is implemented [148]. The presence of these oxidizing agents at high temperatures generates

reactions with the biochar structure. While the activation with steam and CO_2 is an endothermic process and therefore easy to control (Eqs. (1.8)–(1.10)), the activation with oxygen is exothermic (Eq. (1.11)) and therefore more difficult to control. For this reason, such activation is not common [149]. Regarding the development of porosity, the activation by physical treatments generates pores in the range of micropores and a fraction of mesopores [142, 150–152].

When activated with carbon dioxide ($\Delta H = 159 \text{ kJ mol}^{-1}$)



When activated with steam ($\Delta H = 117 \text{ kJ mol}^{-1}$)



At high temperatures, water gas shift reaction ($\Delta H = -41 \text{ kJ mol}^{-1}$) may also occur:



When activated with air ($\Delta H = -406 \text{ kJ mol}^{-1}$)



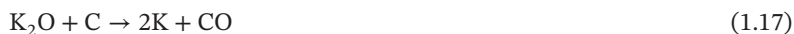
1.3.2.2 Chemical Activation

The chemical activation of biochar refers to biomass impregnation with an activating agent, such as ZnCl_2 , H_3PO_4 , NaOH , KOH , and K_2CO_3 . The function of the activating agents is to increase the porosity through dehydration and degradation processes, which occur at lower temperatures compared to physical activation [153, 154]. Generally, in lignocellulosic precursors, KOH , H_3PO_4 , ZnCl_2 , and K_2CO_3 are commonly used as activating agents. There are differences in the porosity developed when using an activating agent with respect to another. In biochars activated with KOH and ZnCl_2 , microporosity prevails. While those activated with H_3PO_4 and K_2CO_3 , a significant portion of pores are mesoporous [155–158]. Not all activating agents work using the same mechanism. For instance, the mechanism of an acid agent (H_3PO_4), an alkali (KOH), and a salt (K_2CO_3) are described below.

Chemical reactions when activated with KOH



Chemical reactions when activated with K_2CO_3



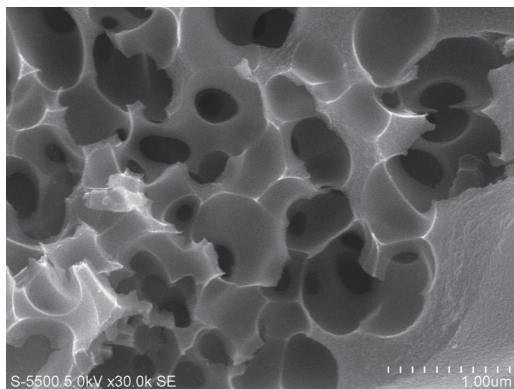


Figure 1.10 Biochar from *Agave angustifolia* activated with K_2CO_3 .

Activation with H_3PO_4 : This acid has its main effect before the pyrolysis of biomass with less effect in carbonization. During the impregnation period, this acid interacts with biomass oxygen functional groups, allowing the bond breaking between lignin and cellulose. During pyrolysis, H_3PO_4 increases the thermal stability, promoting a higher carbon yield and the dehydration at 200 °C. This aids to obtain more stable aromatic structures. However, new chemical bonds between phosphorus and carbon can be formed [88]. The pores caused by this activating agent are mainly micro- and mesoporous [150, 159].

Activation with KOH: This activating agent acts through two mechanisms. The first involves microporosity formation because of the addition of KOH to the biomass that causes changes in the structure. The second mechanism occurs during the pyrolysis, and it is based on the superficial atom gasification from biochar. The porosity resulting from the activation of KOH as an agent remains in the order of the micropores (Eqs. (1.12)–(1.14)) [150, 160].

Activation with K_2CO_3 : The first step of this activation results in the decomposition of a fraction of K_2CO_3 into CO_2 and K_2O (Eq. (1.15)). The other fraction of K_2CO_3 reacts with carbon atoms to form K_2O and CO (Eq. (1.16)). Finally, K_2O obtained by both mechanisms reacts with carbon to obtain metallic potassium and CO (Eq. (1.17)) [156]. An example of biochar activated with this carbonate is shown in Figure 1.10.

1.3.2.3 Pseudocapacitors

This branch of SC is not assembled with carbon-based electrodes, and it is out of the scope of this chapter. However, pseudocapacitive materials can be used in combination with a carbon material that stores energy through the double layer to form hybrid supercapacitors (HSCs). Pseudocapacitors are those SCs that work by means of fast faradaic processes that involves electron transfer mechanism that take place on the electrode–electrolyte interphase [161]. Pseudocapacitors have similar electrochemical signature than that of an electric double-layer capacitor (EDLC). However, the energy storage phenomenon occurs due to reversible faradaic processes of rapid kinetics. In addition, the response of a pseudocapacitor exhibits a linear dependence of the charge and voltage [162]. In summary, the differences between the storage

by means of the double layer and pseudocapacitive processes are the double layer is a nonfaradaic process, whereas pseudocapacitance is faradaic and usually stores more energy than the double layer. Additionally, the pseudocapacitance is limited for kinetic reasons and it presents a restricted potential range [163].

1.3.2.4 Hybrid Supercapacitors

HSCs receive this name because they are a combination of EDLC and faradaic devices. HSCs employ a battery-like electrode, which provides high energy, and a capacitor-like electrode, which provides power. The purpose of combining these two types of electrodes in the same device is to deliver high energy, in a combination with high power. Hybrid systems can be formed of pseudocapacitive oxide and capacitive carbon materials, or lithium-insertion electrodes and capacitive carbon materials [131, 164]. Among the carbon materials that are usually implemented as a capacitive electrode in the assembly of HSCs are graphene, carbon nanotubes, and activated carbon. With respect to the faradaic electrode, this is usually based on transition metal oxides, hydroxides, sulfides, conductive polymers, among others [165].

Some examples are HSCs assembled with transition metal oxides of Mn and Co (MnCoO_4) and activated carbon [166], hydroxides and chitosan-derived carbon [167], sulfides (CoNi_2S_4) and activated carbon [168], conducting polymers and graphene [169], lithium-based materials and activated carbon [170], among many others.

1.4 Computational Simulation of Nanocarbon Structures from Lignin-Derived Materials with Potential Application in Energy Storage Devices

1.4.1 Computational Study of Lignin from Different Computational Approaches

The study of lignin from a theoretical perspective has been the subject of intense research. As it was previously discussed above, it may be extended to multiple applications, including storage and energy conversion when transformed into carbon structures. Qin et al. [171] used quantum theoretical methodologies to study structural changes in lignin at the phosphoric acid-acetone process and its related reactions. Qin and coworkers initially studied a lignin model (see Figure 1.11) using a reactive potential at the ReaxFF level [172]. From the relaxed structures, the calculations by density functional theory (DFT) were developed with the generalized gradient approximation (GGA)/PBE functional and with the DNP [173] basis set and using the DMol³ computational code [173]. Solvation effects were accounted in the electronic structure calculations with reference to the dielectric constants and the polarizable continuum method. Additionally, the search of transition states was also performed to explore lignin reactivity in the simulated process with the aid of the quadratic synchronous transition (QST) method [174].

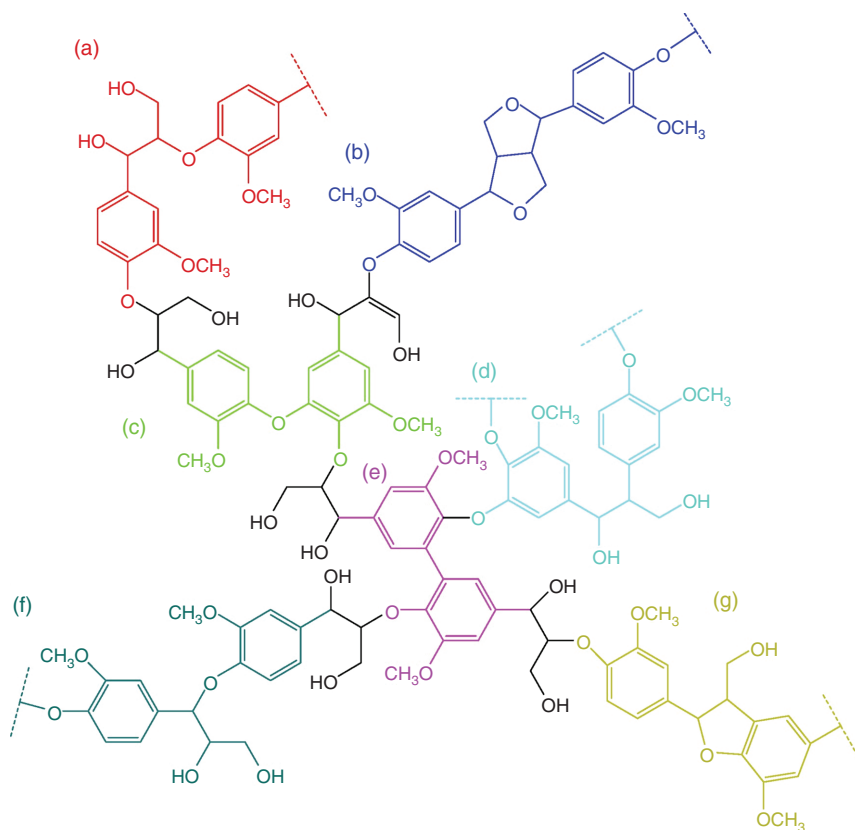


Figure 1.11 Optimized lignin model to show the different bonding: (a) β -O-4, (b) β - β , (c) 4-O-5, (d) β -1, (e) 5-5, (f) α -O-4, and (g) β -5. Source: Qin et al. [171], CC BY 4.0.

As it was previously discussed, lignin corresponds to a macromolecule formed of three hydroxycinnamyl alcohols: sinapyl alcohol, coniferyl, and *p*-coumaryl (see Figure 1.12). For notation, such monomers are known as syringyl (S), guaiacyl (G), and *p*-hydroxyphenyl (H). After incorporated into a lignin polymer, they are known as monolignols [175]. Such monolignols are depicted (see Figure 1.12). Each group is highly reactive during the polymerization with the following hierarchy: $S < G < H$.

In this respect, there is a directionality in the bonding at sites 3 and 5 (see Figure 1.12), which yielded stronger C—C bonds than those of C—O pairs. Furthermore, a wide range of possibilities could rise for the C—C and C—O bonds. The most common is the β -O-4 alkyl aryl ether. Nevertheless, the bonds β - β , β -5, β -1, and 5-5 could also be present (see Figure 1.12b). When the lignin polymer was formed, the β -O-4 and β - β bonds were responsible to form linear chains, while the branching could be attributed to α -O-4, 5-O-4, and eight-membered rings of dibenzodioxin [176, 177]. Consequently, the structure of lignin was of high relevance because a deep knowledge of the building blocks forming lignin could be fundamental to tailor materials, with desirable applications in biofuel production or

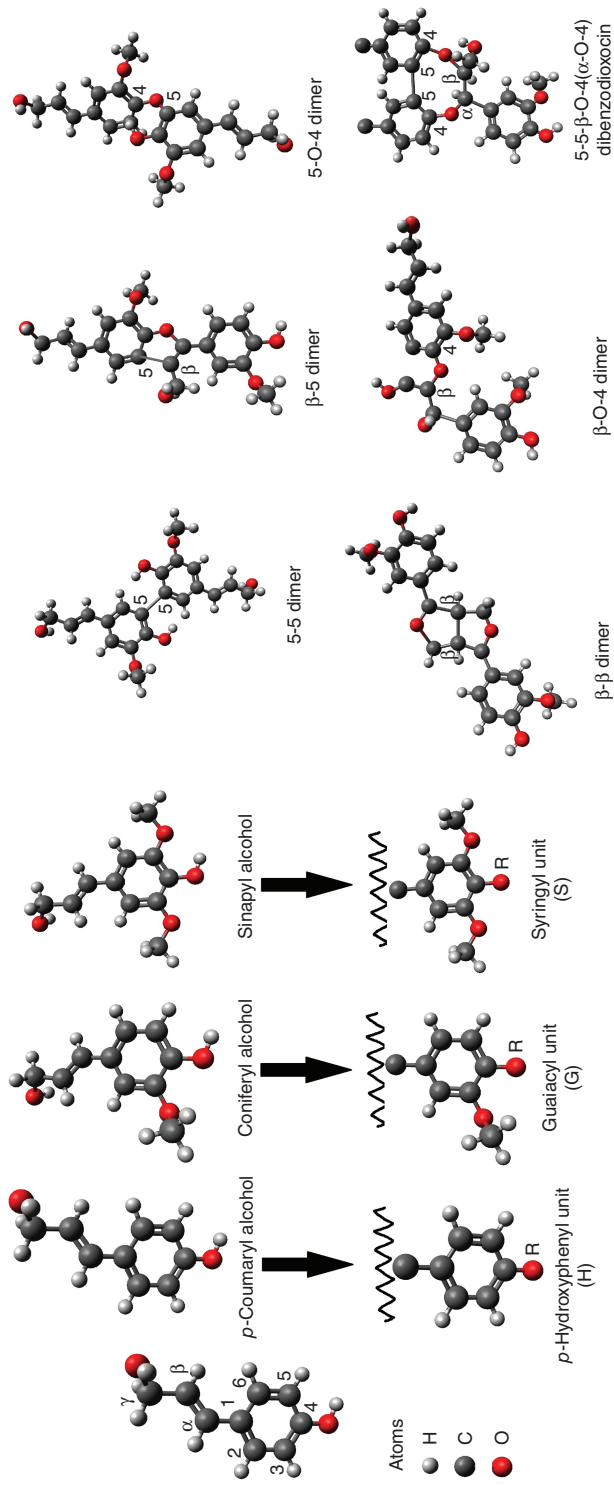


Figure 1.12 Monomers of *p*-coumaryl, coniferyl, and sinapyl alcohol (monolignols). After incorporation to lignin, they are referred to as *p*-hydroxyphenyl (H), guaiacyl (G), and syringyl (S). Source: Adapted from Sangha et al. [175].

on its incorporation into molecular devices, such as those for energy storage when transformed to carbon by any thermochemical process.

Intermolecular interaction during lignin pyrolysis is widely studied theoretically because lignin and formation of derived products are simultaneously presented in the real pyrolysis process. The principal mechanism of pyrolysis is the unimolecular decomposition [178]. Jiang et al. performed a theoretical study using M06-2X/6-31+G(d,p) functional using Gaussian 09 program [179] and experiments of analytical pyrolysis gas and chromatography/mass spectrometry (Py-GC/MS) to evaluate the intermolecular interaction. The results showed a strong interaction of radicals, lignin, or derivated products through H-subtraction reactions and concluded that the unimolecular decomposition is not the dominant mechanism in the lignin pyrolysis [178] and it may affect the pyrolysis process.

An alternative to simulate the pyrolysis process, evolving longer time scales and in which no bond formation or breaking is necessarily involved, the implementation of molecular dynamics (MD) simulations based on Newtonian classical mechanics, is an adequate choice. The processes that involve oxidative coupling require the exclusive use of quantum mechanical calculations based on the resolution of the many-body Schrödinger equation, with the aid of DFT, as the most reliable alternative. Massive systems with several hundreds of atoms may be easily tractable from the theoretical methods, within an affordable time, but the handling of smaller sized systems is the adequate approach in the implementation of DFT calculations. A comprehensible review on such methodologies has been developed by Cramer [180]. Moreover, there are also alternative theoretical schemes, which have given acceptable results, such as the semiempirical methods, comparable with DFT, but at a faster rate. This could be achieved after (i) neglecting the electron–electron interaction (and excluding dispersive forces) and (ii) introducing fitting parameters that consider electron correlation (for instance, PM3 [181] and AM1 [182], PDDG1PM3 [183] methods). Therefore, the study of the rotation in the C—C or C—O bonds should be analyzed by searching conformers. This can be studied with semiempirical or MD simulations and genetic algorithms to scan lower energy conformers. Nevertheless, the functionals recently developed incorporate dispersion effects at a high degree of accuracy and can be successfully implemented in the study of molecular lignin, as it has been shown somewhere else [184, 185].

In this direction, DFT methodologies have been used to aid in the understanding of unknown properties of lignin-related systems such as thermodynamic control of lignin biosynthesis, in which it was elucidated that the number of lignin bonds should be correlated with their thermodynamic stability. Moreover, DFT has also aided to understand the spin distribution hypothesis, which stands that the lignin sites with a larger number of unpaired electrons are susceptible to a higher reactivity. To analyze the electronic structure properties from lignin monomers (monolignols) and related compounds, DFT was required. Durbeej et al. [186–188] performed a theoretical study at the DFT/Becke-3-Lee-Yang-Par (B3LYP) [189] level of theory, by simulating solvent effects with the polarizable continuum approach in order to study oxidative coupling on coniferyl monomers. It was disclosed that a large number of unpaired electrons are allocated at the O₄ phenoxy radical. This gave insights into the

preservation of β -O-4 bonding observed in lignin. Additionally, an energy ranking was stated in the following order: β - β < β -5 < 5-5, and they consistently found that the strongest bond was β -O-4.

Following this same level of theory, Huang and He [190] performed a DFT study at the B3LYP/6-31G(d,p) level to study the behavior of lignin pyrolysis and the principal products. They used a model of lignin dimer of α -O-4 linkage (see Figure 1.13). Three reaction pathways were proposed for C_α -O, O-CH₃, and C_α -C $_\beta$. The major channel of pyrolysis was a reaction of C_α -O bond. The O-CH₃ bond is competitive with the C_α -C $_\beta$ reaction mechanism of pyrolysis. The bond dissociation energies from 177.4 to 396.6 kJ mol⁻¹ followed the order: C_α -O < O-CH₃ < C_α -C $_\beta$ < O-H < O-C_{aromatic} < C $_\beta$ -OH < C_α -C_{aromatic} and the products obtained from pyrolysis (see Figure 1.13) were phenolic compounds (guaiacol [8], *p*-hydroxyphenyl-acetaldehyde [5], *p*-hydroxyphenyl-ethanol [7], and 2-hydroxybenzaldehyde [13]).

Beste et al. [184, 185, 191, 192] studied lignin pyrolysis with DFT approaches by considering lignin-related models. They considered phenethyl phenyl ether (PPE) to study reactivity for hydrogen abstraction. It was shown that it could be depleted in the pyrolysis process from the α and β positions. The possibilities to obtain smaller chains in the pyrolysis were also developed by assessing the enthalpies of dissociation of C-C and C-O pairs.

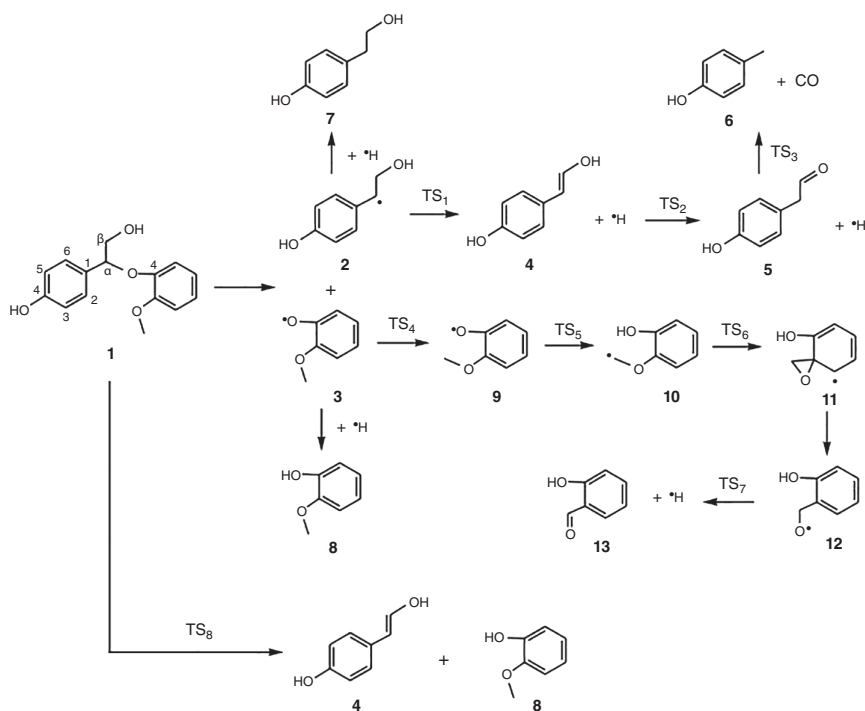


Figure 1.13 Reaction pathways proposed for the homolytic cleavage of C_α -O bond. Source: Huang and He [190], with permission of Elsevier.

The discovery of covalent attractions was identified in the study of a double-stranded lignin chain. Such interactions were determinant in the monolignol orientation. Combined theoretical/experimental studies have also been performed for monolignols in the gaseous phase to show that allyl chains were contained in fixed positions, in which the hydroxyl group interacted with the π -electrons of the vinyl group. The phenolic hydroxyl group of coniferyl and sinapyl gave rise to hydrogen bonding with the methoxy groups.

As it was previously suggested, the use of MD simulations defeated the computational barrier of DFT calculations since a much larger number (about 105) of atoms could be accounted in the computations. This may be achievable because of the incorporation of a force field that does not necessarily include an exhaustive treatment of electron correlation. In this direction, MD simulations based on the Chemistry at Harvard Molecular Mechanics (CHARMM) force field were performed on the β -O-4 guaiacyl dimer in a water solvent environment. It was disclosed that the intermolecular bonding was more likely to be formed than the intramolecular bonding [193]. Those results were supported by experimental evidence with nuclear magnetic resonance (NMR) spectroscopy, showing transient intermolecular hydrogen bonding [194].

Besomes and Mazeau [195] also studied the interactions lignin–cellulose. The cellulose structure was responsible for changes in the geometry of lignin phenol rings upon adsorption. On the other hand, Besomes and Mazeau [196] studied the adsorption of cellulose on a reduced molecular model of lignin of β -O-4 guaiacyl polymers, in which lignin adsorbed with flat orientations on cellulose. It was found that van der Waals (vdW) interactions ruled the adsorption.

Moreover, a CHARMM potential for lignin was developed [197] with an analogous methodology as that for proteins and nucleic acids [198]. Reduced models of lignin (methoxybenzene and *p*-hydroxyphenol) were used to accelerate the process. Such CHARMM potential was developed with descriptors obtained from quantum chemical parameters. Combined experimental/MD simulation studies have also been performed by using small-angle neutron scattering (SANS) to analyze the molecular geometry of softwood lignin systems [199] (see Figure 1.14). It was

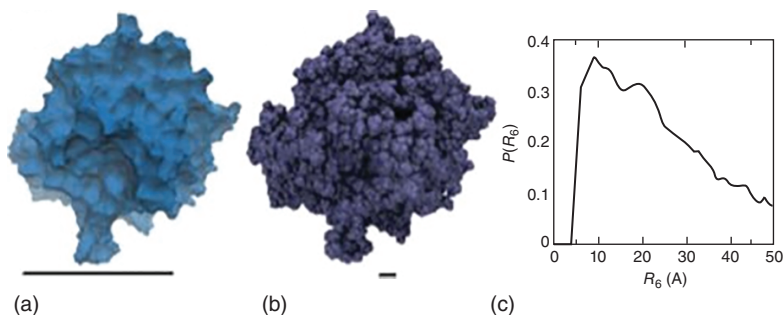


Figure 1.14 (a and b) Lignin molecular surfaces obtained by a probe molecule of 4.0 Å at different radii of gyration and (c) probability function of the radius in a sphere, which was adjusted to the surface depicted in (b). Source: From Petridis et al. [199], with permission from the American Physical Society.

concluded that the geometry of lignin polymers was highly sensitive to temperature. Furthermore, as it was previously stated, the use of MD simulations was preferable to speed up calculations in massive systems. This has also been scaled up in high-performance computing, with a large number of processors (approximately 30 000). Further reading on the interactions lignin/cellulose in aqueous solutions may be found somewhere else [200, 201].

Regarding the study of the geometry of lignin, stiffness of bamboo fibrils was also analyzed [202] because the strength of this fiber is similar to that of steel or concrete. Its molecular structure was formed of cellulose microfibrils with hemicellulose and lignin, coexisting in a lignin carbohydrate complex (LCC). The elastic moduli in these structures were studied and also the adsorption energies among the components. The results revealed that hemicellulose presented better mechanical properties than those of lignin (see Figure 1.15). Moreover, lignin was more susceptible to be adsorbed on the cellulose microfibrils. It was also disclosed that vdW effects between lignin and cellulose ruled the attraction. Furthermore, the strong adherence of lignin to cellulose microfibrils was due to the vdW attraction forces with lignin and cellulose. Additionally, the weakest interaction in the cellulose structure was found in the interface of the amorphous region.

That study was performed by using a force field for the condensed-phase optimized molecular potentials for atomistic simulation studies (COMPASS) [203], which included thermal, structural, and mechanical properties of a set of compounds, such as cellulose [204]. The modeling considered vdW effects and nonbonded interactions, which were given by the combination of Coulomb attractions (Eelec) and the Lennard-Jones (LJ) function for vdW attractions (EvdW). This scheme has also shown to adequately describe hydrogen bonding.

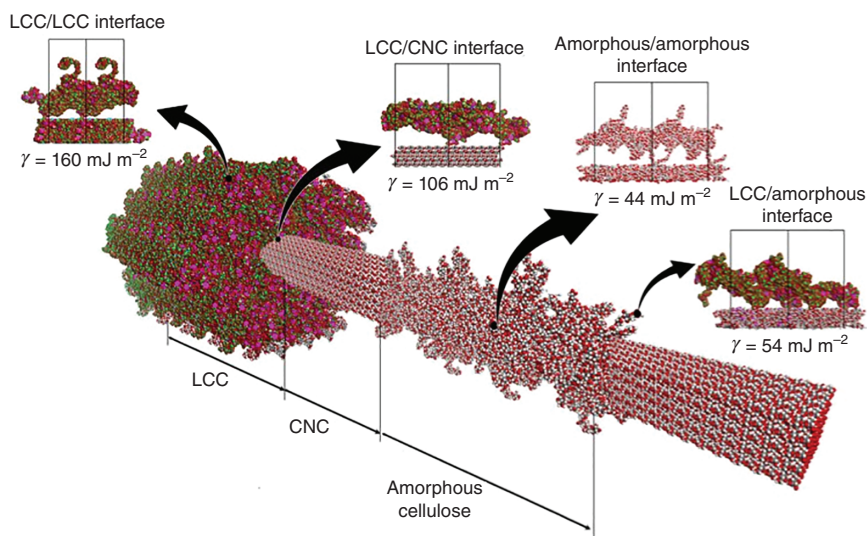


Figure 1.15 A molecular model representing the bonding among lignin and cellulose of a bamboo fiber. The weakest bonding is at the amorphous region, and it may probably give the adhesive properties to the bamboo fibrils. Source: Youssefian and Rahbar [202]. Springer Nature. CC BY 4.0.

1.4.2 Computational Studies of Lignin Through Pyrolysis-Simulated Molecular Dynamics

The range of applications of lignin-related systems has allowed to explore its electronic structure properties. For instance, Janesko [205] studied the interactions among lignin and cellulose with ionic liquids in order to elucidate possible rates to synthesize fuels and chemical feedstock from biomass. In that work, dispersion-corrected density functional theory (DFT-D) was used to analyze the interactions among an ionic liquid and a lignin/cellulose system. It was

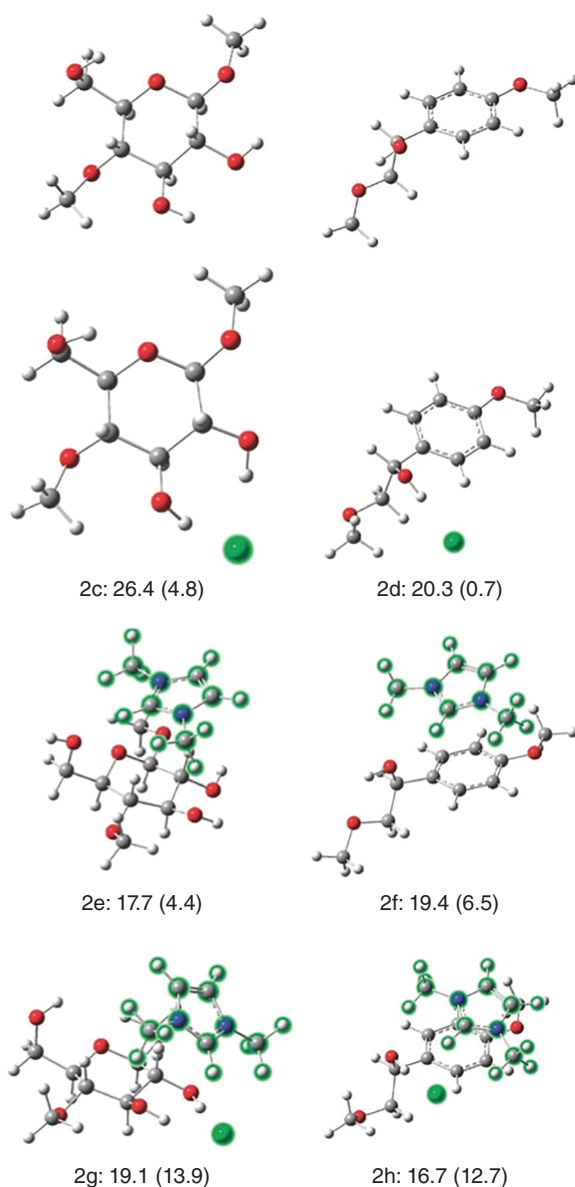


Figure 1.16 The atoms highlighted in green represent the ionic liquid. In the top side of the figure, the relaxed molecular models of Glu and LigOH are shown. The second, third, and last rows represent their compounds with Cl^- , mmim^+ , and single $[\text{mmim}][\text{Cl}]$ ions. Additionally, the binding enthalpies are shown, as computed with the presence of a solvent. Source: Janesko [205], with permission of Royal Society of Chemistry.

considered imidazolium chloride anions, (1,4)-dimethoxy- β -D-glucopyranose, 1-(4-methoxyphenyl)-2-methoxyethanol as the molecular systems for the ionic liquid; cellulose and lignin, respectively. It was reported that lignin presented a strong π -stacking with the ionic liquid (see Figure 1.16). This could be used as a tool to tune the relative solubility of cellulose and lignin with the aid of ionic liquid cations. The study was carried out by using Gaussian 09 computational code [179] with the B97-D dispersion-corrected exchange–correlational functional [206] and the 6-311++G(2d,2p) basis set. The calculations were performed in an aqueous environment within the integral equation formalism-variant polarizable continuum model [207]. Moreover, the PM6 [208] semiempirical method, the Couple Cluster (CCSD (T)), and the Moller–Plesset many-body perturbation theories at second order were also implemented in the computations to benchmark the methodologies.

In the search of applications of lignin-derived materials, the simulated pyrolysis of lignin monomer rings has been studied. That is, Zhang et al. [209] studied such systems with MD simulations at the ReaxFF level [210]. A massive model of 15 920 atoms was used based on Adler’s lignin softwood model [211]. During the pyrolysis simulations, the monomer aryl rings of α -O-4, β -O-4, α -O-4, and β -5

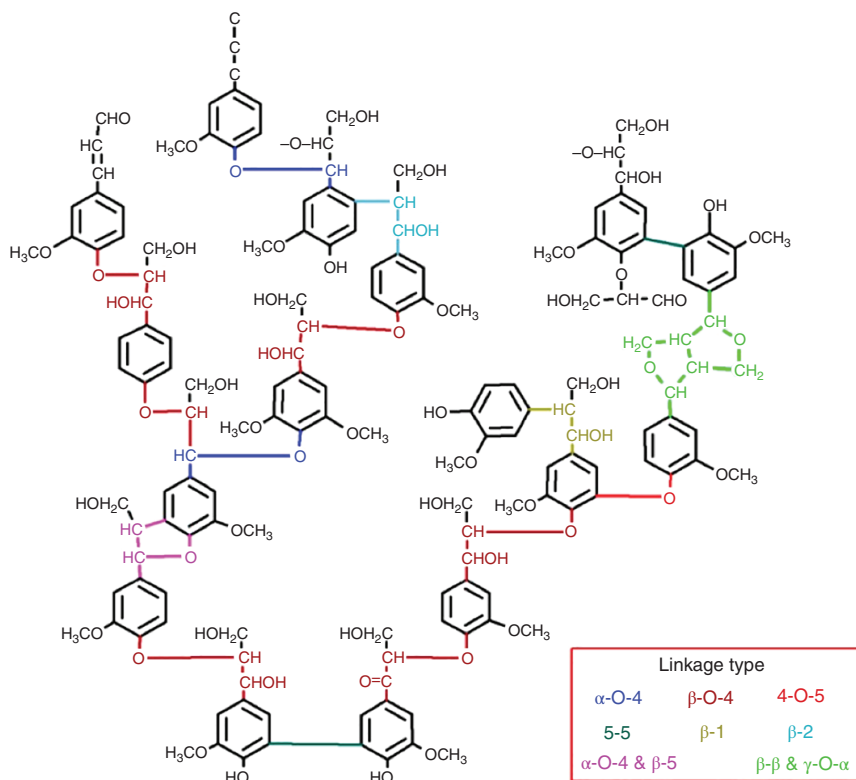


Figure 1.17 Molecular model of lignin in accordance with Adler’s model. Different bondings are represented with colors. Source: Zhang et al. [209], American Chemical Society.

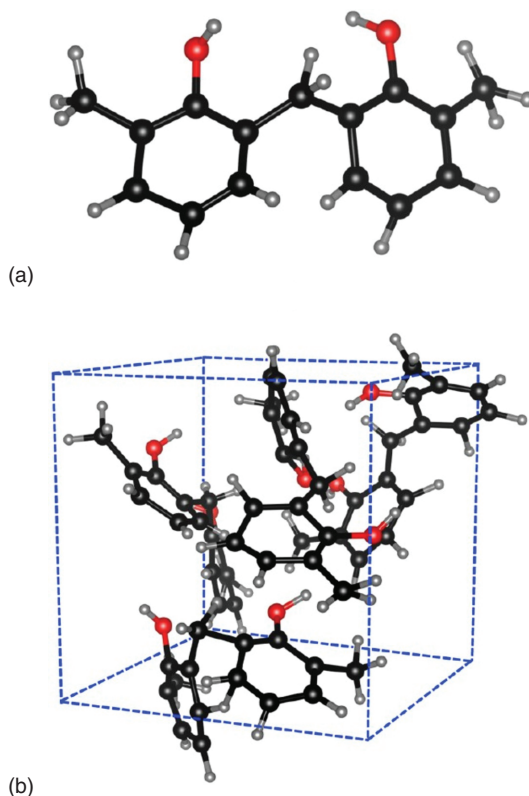
mainly presented a C_α/C_β ether bond breaking (see Figure 1.17) at the first reaction pathway. Moreover, in the bonds β - β and γ -O- α , the bond breaking in the C_α -O ether and its aryl ring were also predominant. The simulated pyrolysis also reported ring opening as a consequence of the breaking of other bonding such as 4-O-5, 5-5, β -1, β -2, and β -5.

Intermediate compounds giving rise to stable aryl ring opening were addressed to phenoxy radicals, three-membered rings, bridged five-membered rings, and six-membered rings. It was also concluded that the breaking of the bonds α -O-4 and β -O-4 could be responsible for the rising of adjacent bonding with the phenoxy radicals. Additionally, the first stage in the pyrolysis-simulated reaction exposed hidden intermediate complexes. This is an important issue in the control of aryl ring opening. It could be directly related to the formation of aromatic compounds used in energy conversion and storage. Such results could also aid to tailor lignin-derived materials to obtain aromatic chemical products for diverse applications. The computations were performed with ReaxFF [210] on a massive model of 40 lignin macromolecules, as dictated by Adler's model (15 920 atoms). A graphics processing unit (GPU) version of the Reax code [212] was implemented in this study to speed up the calculations. The MD simulations were carried out with the NVT ensemble with a 0.4 K ps^{-1} heating rate starting from room temperature up to 2100 K. The calculations were performed with the Reax module implemented in large-scale atomic/molecular massively parallel simulator (LAMMPS) [213] computational code.

The theoretical study of lignin has also been extended on the computation of the electronic structure properties of conifer alcohol as a molecular model system of lignin. Such model was used to analyze its antioxidant potential for hydrocarbons, such as petroleum asphalt. In this respect, Pan and Cheng [214] used *ab initio* MD calculations to simulate the interaction between both species. The calculations revealed that the radicals of asphalt are responsible for the formation of agglomerates or decomposition of asphalt. An highest occupied molecular orbital (HOMO)-lowest unoccupied molecular orbital (LUMO) gap of lignin, which was larger than that of the asphalt, was not recommendable to protect it from decomposition because no antioxidant activity was observed. In that respect, the lignin model should previously be evaluated on its hydrophobicity and compatibility with the corresponding hydrocarbon. This study could be used as a tool to determine lignin models for antioxidant capacities in hydrocarbons.

In a more general context, pyrolysis of phenolic compounds has also been studied with analogous systems [215] to those forming the lignin macromolecule (see Figure 1.18). That is, Qi et al. [215] performed a comparative work in which three different theoretical approaches were explored: DFT, self-consistent charge density functional tight-binding (SCC-DFTB) and MD at the ReaxFF level. A generic phenolic polymer was used as a model system (see Figure 1.18), namely, the cross-linked phenol formaldehyde resin molecule. The pyrolysis was simulated from an initial temperature of 2500 K until reaching a final temperature of 3500 K. The reactivity giving rise to subproducts and char were thoroughly examined. After comparing all methodologies, it was reported that the same subproducts were obtained but with

Figure 1.18 (a) Phenol resin molecule; and (b) simulation box with a total of 132 atoms. Source: Qi et al. [215], with permission of American Chemical Society.



different yields. The DFTB methodology dramatically overestimated CO release and it underestimated free hydrogen formation and hydrocarbons, as compared with the DFT methodology. In the case of ReaxFF, free hydrogen was also underestimated with respect to DFT. The same behavior was observed for fused carbon rings. Particularly, the formation of five- and six-membered rings was identified at 2500 K. The formation of H₂O, CO, and char was analyzed. Additionally, the pyrolysis was also studied with quantum nuclear effects, which could be directly related to its chemical equilibrium. The char analysis deduced the rising of the carbon five- and six-membered rings. Nevertheless, the rising of rings with five carbon members and one oxygen member were also identified. This behavior was expected to result in chemical stabilization of the structure, which could reduce the formation of graphitized structures in the resulting char after pyrolysis. This may also be associated with the physicochemical properties of the char.

The DFTB calculations in that benchmark study were performed with the SCC-DFTB [216], as implemented in the DFTB+ computational code [217]. DFT MD was carried out with the PW91 functional [218] with the Vienna ab initio simulation package (VASP) computational code [219]. ReaxFF was used with the Chenoweth et al. force field [172] by using LAMMPS [213] computational code. The simulations were performed in a box with 132 atoms. All calculations were done in accordance with the NVT canonical ensemble with the aid of a Nosé–Hoover thermostat.

The pyrolysis of lignin was also analyzed by Zhang et al. [220] at the ReaxFF level with a GPU-based version (GMP-Reax). Adler's molecular model was implemented, and the simulated pyrolysis was performed from room temperature to 2100 K and from 500 to 2100 K. The massive lignin model under study contained 15 920 atoms. The simulation was performed in three stages, and the reaction mechanism in the aryl monomers and substituents of propyl chains and methoxy was also studied. At the beginning of the simulation, the α - and β -O-4 were broken. Moreover, in the subsequent part of the simulation, the breaking of all bonding was revealed. During this stage, the formation of propyl and methoxy was also observed. Finally; at the third stage, the rising of heavy pyrolysates was reported, which was addressed to the mixing of five-, six-, and seven-membered rings. Furthermore, the formation of small molecules during the computations revealed close agreement with that observed in experimental works. The final stage was also characterized with the absence of C6–C23 species, which were converted into C0–C5 species. Char formation was also observed from the presence of carbon clusters with 160 or more atoms (C160+) and also molecular hydrogen. This is mainly characterized by the formation of five-, six-, and seven-membered rings. In this respect, it would be straightforward to use this methodology to explore physicochemical properties in char formation in order to elucidate potential applications in electrodes for

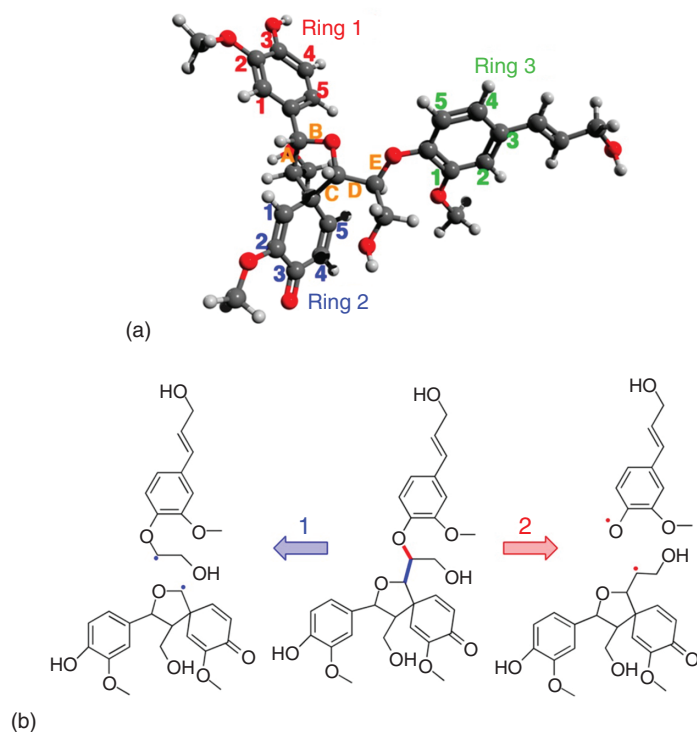


Figure 1.19 (a) Molecular model of lignin spirodienone with the rings involved in the study and (b) reactive route of the linkages in the molecular model for D and E bonds (1 and 2, respectively) Source: Mar and Kulik [221], with permission of American Chemical Society.

supercapacitor applications. Consequently, this pioneer work represents a key starting point to further study phenomena by computational methodologies related to lignin pyrolysis. In that study, the simulation box was initially relaxed by using the NPT ensemble at 300 K and 760 Torr. The simulated annealing was led to a target temperature of 800 K with the NVT ensemble. The simulation box size was 58 Å, and the Berendsen thermostat was used.

Mar and Kulik [221] performed *ab initio* MD simulations in hundreds of possible reaction coordinates. In that study, lignin polymerization was analyzed in a simulated pyrolysis process. The model system under study was the spirodienone lignin (see Figure 1.19a). Such system was chosen because approximately 10% of the total lignin in softwoods has been observed. Mar and Kulik identified some favorable pathways for polymerization (see Figure 1.19). The most stable fragments in the spirodienone lignin formed small energy barriers in C—C bonding, allowing the structure to be susceptible for lignin depolymerization. This may also aid to tailor novel catalytic materials. TeraChem computational code [222] was used at the ω PBEh level of theory. The search of transition states was performed with the methodology given by the climbing image nudged elastic band (NEB) [223].

1.5 Tailoring Nanocarbon Structures to Enhance the Performance of Electrodes in Supercapacitors

Materials based on lignin and subjected to pyrolysis conditions have also been analyzed to deepen into the structural properties of char formation. That is, Muñiz et al. [86] performed a pioneer study to explore the capabilities of carbon char for energy storage applications. In this direction, the quest of novel nanoporous carbon materials coming from biomass resulted in a breakthrough. In that work, a combined experimental and theoretical study was carried out, in which macromolecular models of lignin (Adler's model), cellulose, and hemicellulose were considered. The simulated pyrolysis was modeled at the ReaxFF level in massive model systems (see Figure 1.20a–c) for the three lignocellulosic components. The annealing was implemented from room temperature to a target temperature of 1280 K in order

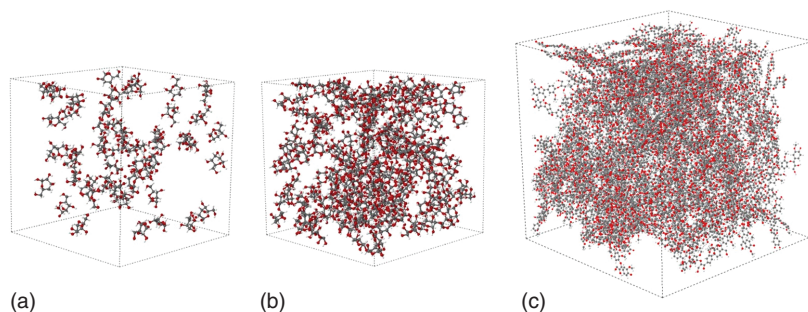


Figure 1.20 Simulation boxes of (a) cellulose, (b) hemicellulose, and (c) lignin. Source: (a, b) Muñiz et al. [224]. Elsevier. CC BY 4.0. (c) Muñiz et al. [86], with permission of Elsevier.

to simulate the experimental conditions. The annealing process remained constant during a period of time and the systems were further stabilized until reaching room temperature. The key goal of the study was to evaluate the resulting char to identify structural properties that could be of interest to implement carbon systems for supercapacitors or batteries. Moreover, chemical reactivity of the lignocellulosic components was thoroughly analyzed using the PBE functional. Isolated molecular systems were evaluated via the Fukui indexes of electrophilic attack. It was found that cellulose and hemicellulose were highly reactive at the carbon sites, while lignin appeared to present low reactivity at all carbon rings forming the macromolecule. Such theoretical results are in agreement with evidence from the laboratory, in which lignin content on biomass determined the yield of carbon.

The simulated annealing was modeled in the temperature ranges previously discussed and the formation of subproducts, such as H_2O , H_2 , and CO_2 , was identified (see Figure 1.21). The formation of char (C_{300+} and C_{3500+}) was mainly identified after 700 K for the lignin pyrolysis. The resulting nanoporous structures were characterized using radial distribution functions (RDFs), which were intended to quantify the number of C—C bonding pairs in the amorphous carbon structure.

Because the study was performed for different lignin densities and heating rates, the RDF profiles followed a tendency that showed characteristic peaks located at 1.4 and 2.5 Å, yielding a hybridized sp^2/sp^3 structure with graphitized morphology. Additionally, X-ray diffraction (XRD) of *Agave angustifolia* was also performed in that study by using a pyrolyzed sample, with the conditions obtained at a solar furnace with the experimental conditions given in our group [112], as it was previously discussed. A fast Fourier transform (FFT) was subsequently used to obtain experimental RDF profiles of char with densities close to 1 g cc^{-1} (see

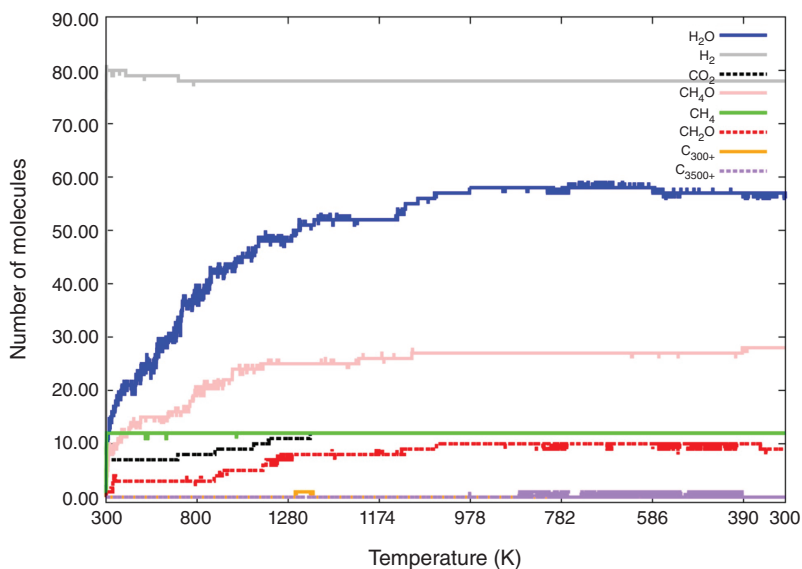


Figure 1.21 Simulated lignin pyrolysis at a heating rate of 0.005 K fs^{-1} . The density of the nanoporous carbon amounts to 0.4715 g cc^{-1} . Source: Muñiz et al. [86], with permission of Elsevier.

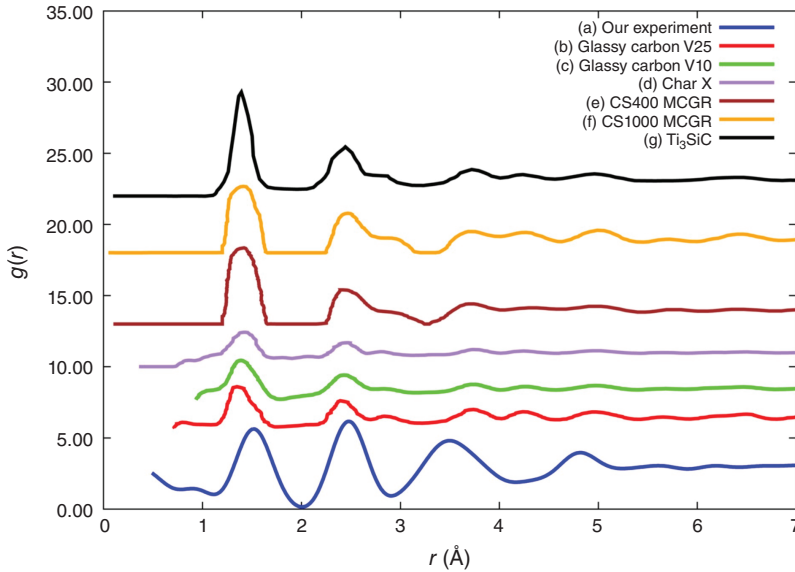


Figure 1.22 RDF profiles of different nanoporous carbon materials. Note that (a) corresponds to the biomass analyzed in our experiment; (b) glassy carbon V25, (c) glassy carbon V10, (d) char-X, (e) CS400 MCGR, (f) CS1000 MCGR, and (g) Ti_3SiC_2 . Source: Muñiz et al. [86], with permission of Elsevier.

Figure 1.22). The characteristic peaks were also reproduced, disclosing the atomistic structure of char nanoporous carbon coming from lignocellulosic components. This is shown in Figure 1.23. Additionally, PSD theoretically obtained was also evaluated, showing that those nanoporous structures close to a density of 0.8 g cc^{-1} reported maxima around 15 Å . According to Pandolfo and Hollenkamp [225], such size distribution is highly preferable to yield large double-layer capacities in supercapacitor applications, as it was previously reported in carbon aerogel with H_2SO_4 . Moreover, the graphitized structure along with PSD could represent descriptors in the in silico design of nanoporous carbon electrodes coming from biomass.

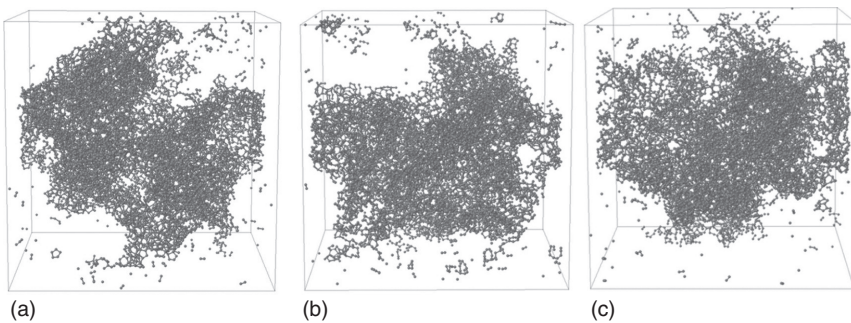


Figure 1.23 Simulation boxes of char after pyrolysis. The simulations were performed at (a) 0.1 K fs^{-1} , (b) 0.0196 K fs^{-1} , and (c) 0.005 K fs^{-1} . Source: Muñiz et al. [86], with permission of Elsevier.

That is, depending on the biomass origin, it would be possible to select pyrolysis routes with controlled conditions that could give us optimal parameters to obtain nanoporous structures in one of the alternatives of controlled pyrolysis. Additionally, Muñiz and coworkers considered two different approaches to model lignin pyrolysis: (i) The evaluation of reactivity of all atomic sites during the annealing and (ii) the detachment of O and H atoms at the second part of the simulated pyrolysis. According to the RDF profiles, it was concluded that the last approach was not physically feasible and excluded the reactivity of the lignin components. The additional structural data of the final simulated pyrolysis were also collected and analyzed by Muñiz et al. [224]. Such data could be used to model further supercapacitor electrodes, in which the nanoporosity is crucial to determine the capacitive properties and performance. In those works, the ReaxFF module of LAMMPS code was employed, using NVT ensemble and Kim's reactive force field potential [226]. The simulated pyrolysis of lignocellulosic components has not been performed. This could be imperative to elucidate the role of cellulose and hemicellulose gasification in the remaining structure of pyrolyzed derived lignin products. Theoretical calculations on the dependence of three components during pyrolysis are being performed in our group.

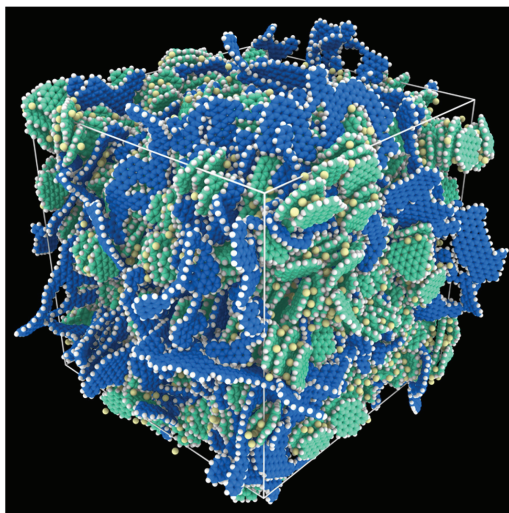
1.5.1 MD to Aid the Design of EDLCs

The performance of EDLCs could be improved if the electrode–electrolyte interactions are enhanced in the device. Because of this fact, the MD could give tendencies to achieve this target, for instance, through the optimization of parameters involved in the performance of supercapacitors. As previously suggested, electrode geometry could be modified with MD. Thus, the pore size and topography of a carbon electrode can influence the electric double-layers (EDLs) capacitance [227]. The MD studies of porous materials are based on porosity carbon matrixes that have polyhedral voids, with diverse PSD in their structure [228]. To perform a systematic study, it is necessary to build numerical models with random frameworks of carbon. The Reverse Monte Carlo protocol [229] is a methodology to obtain a structure as that obtained in the laboratory. Consequently, the electrode system could be tailored for MD simulation and to investigate the molecular motion to compare different properties in the geometry, such as PSD, homogeneity, among others.

MD has also been used to study gaseous molecules such as N_2 , adsorbed at the interlayer between the electrode and the electrolyte. It has been performed by simulating the adsorption of dissolved N_2 in an EDL of an aqueous electrolyte near the spherical carbon electrode. The adsorption in the negatively charged electrode increases and decreases under a moderate surface charge density and high surface charge density, respectively [230].

Using MD has also been used to study properties of carbon anodes synthesized from lignin, applied to Li-ion batteries, in which the anode corresponded to the experimental data. Thus, it is possible to show that Li ions did not intercalate among carbon nanocrystallite layers. In this kind of system, it was observed how the Li ions were not localized within the carbon nanocrystallites. Moreover, with the aim to

Figure 1.24 Reaction pathways proposed for the homolytic cleavage of $C_{\alpha}-O$ bond. Source: From McNutt et al. [231], with permission of Elsevier.



identify the migration of the Li ions at interfaces beyond the nanocrystallites based on carbon, a reduced model was simulated within an amorphous carbon matrix using ReaxFF [231]. It could be concluded that the most favorable position to the Li ions is in the region comprising the crystallite and those section of carbon with an amorphous geometry (see Figure 1.24).

1.6 Perspectives for Future Development

One of the routes to explore more insights into lignin structure and reactivity is to use calculations based on coarse-grained methodology, where each atom is represented by a particle. The computing time in this case is significantly reduced, and the properties of lignin may be studied at microsecond time scales. Furthermore, a systematic study combining spectroscopic NMR chemical shifts obtained experimentally, and those computed by DFT methodologies may also bring more clues to understand the spectral assignments and its corresponding origins.

The semiempirical quantum mechanical/molecular mechanical (QM/MM) methodologies could not be neglected because it is possible to incorporate a massive number of atoms simulating lignin and its corresponding environment. That is, it could directly aid to study more realistic models of fibers containing lignin during the pyrolysis process. Such QM/MM methodology may introduce quantum terms only in those bonds participating in the reactive process. Such techniques and their combinations with experimental tools may give more appropriate descriptors that are capable to accurately model lignin during and after the pyrolysis process. This may represent a fundamental tool to design electrodes in supercapacitors with improved properties that allow lignin devices to be competitive with other materials commercially available. The use of *ab initio* methodologies such as DFT and the implementation of MD are key tools that combined with experimental

data may significantly improve the tailoring of lignin-based materials to be used in supercapacitors or batteries.

Acknowledgments

J.M. would like to acknowledge startup funds from Dirección General de Asuntos del Personal Académico (DGAPA-UNAM) under project No. IA102820; the computational infrastructure provided by Laboratorio Nacional de Conversión y Almacenamiento de Energía (CONACYT) under project No. 270810, and the Supercomputing Department of Universidad Nacional Autónoma de México for the computing resources under project No. LANCAD-UNAM-DGTIC-310 and LANCAD-UNAM-DGTIC-370 and the support given by Fondo Sectorial de Investigación para la Educación-CONACYT under project No. A1-S-13294. A.G.L., D.R.L.P., and J.E.P.S. would like to acknowledge the PhD grants provided by CONACYT with Nos. 306891, 738661, and 737320, respectively. The authors would like to acknowledge the financial support given by DGAPA-UNAM under project Nos. IG100720 and IN109319.

References

- 1 Escrivani, G.R., Luna, S.A., and Rodrigues, T.A. (2017). Operating parameters for bio-oil production in biomass pyrolysis: a review. *Journal of Analytical and Applied Pyrolysis* 129 (134–149): 2018.
- 2 Han, X., Guo, Y., Liu, X. et al. (2019). Catalytic conversion of lignocellulosic biomass into hydrocarbons. *Catalysis Today* 319: 2–13.
- 3 Azwar, E., Mahari, W.A.W., Chuah, J.H. et al. (2018). Transformation of biomass into carbon nanofiber for supercapacitor application: a review. *International Journal of Hydrogen Energy* 43 (45): 20811–20821.
- 4 Vassilev, S.V., Baxter, D., Andersen, L.K. et al. (2012). An overview of the organic and inorganic phase composition of biomass. *Fuel* 94: 1–33.
- 5 Hameed, S., Sharma, A., Pareek, V. et al. (2019). A review on biomass pyrolysis models: kinetic, network and mechanistic models. *Biomass and Bioenergy* 123 (December 2018): 104–122.
- 6 Sharma, A., Thakur, M., Bhattacharya, M. et al. (2019). Commercial application of cellulose nano-composites: a review. *Biotechnology Reports* 21 (2018): e00316.
- 7 Klemm, D., Heublein, B., Fink, H.P., and Bohn, A. (2005). Cellulose: fascinating biopolymer and sustainable raw material. *Angewandte Chemie, International Edition* 44 (22): 3358–3393.
- 8 Nechyporchuk, O., Belgacem, M.N., and Bras, J. (2016). Production of cellulose nanofibrils: a review of recent advances. *Industrial Crops and Products* 93: 2–25.
- 9 Gopinath, V., Saravanan, S., Al-Maleki, A.R. et al. (2018). A review of natural polysaccharides for drug delivery applications: special focus on cellulose, starch and glycogen. *Biomedicine and Pharmacotherapy* 107: 96–108.

- 10 Fitria, R.H., Fransen, S.C., Carter, A.H. et al. (2019). Selecting winter wheat straw for cellulosic ethanol production in the Pacific Northwest, U.S.A. *Biomass and Bioenergy* 123 (November 2018): 59–69.
- 11 Dhyani, V. and Bhaskar, T. (2018). A comprehensive review on the pyrolysis of lignocellulosic biomass. *Renewable Energy* 129: 695–716.
- 12 Ahmad, F., Silva, E.L., and Varesche, M.V.A. (2018). Hydrothermal processing of biomass for anaerobic digestion: a review. *Renewable and Sustainable Energy Reviews* 98 (September): 108–124.
- 13 Suhas, V., Gupta, K., Carrott, P.J.M. et al. (2016). Cellulose: a review as natural, modified and activated carbon adsorbent. *Bioresource Technology* 216: 1066–1076.
- 14 Brebu, M., Ucar, S., Vasile, C., and Yanik, J. (2010). Co-pyrolysis of pine cone with synthetic polymers. *Fuel* 89 (8): 1911–1918.
- 15 Huber, G.W., Iborra, S., and Corma, A. (2006). Synthesis of transportation fuels from biomass: chemistry, catalysts, and engineering. *Chemical Reviews* 106 (9): 4044–4098.
- 16 Raveendran, K., Ganesh, A., and Khilar, K.C. (1995). Influence of mineral matter on biomass pyrolysis characteristics. *Fuel* 74 (12): 1812–1822.
- 17 Antal, M.J., Allen, S.G., Schulman, D. et al. (2000). Biomass gasification in supercritical water. *Industrial and Engineering Chemistry Research* 39 (11): 4040–4053.
- 18 Labidi, K., Korhonen, O., Zrida, M. et al. (2019). All-cellulose composites from alfa and wood fibers. *Industrial Crops and Products* 127: 135–141.
- 19 Manimaran, P., Saravanan, S.P., Sanjay, M.R. et al. (2019). Characterization of new cellulosic fiber: *Dracaena reflexa* as a reinforcement for polymer composite structures. *Journal of Materials Research and Technology* 8 (2): 1952–1963.
- 20 de Oliveira, J.P., Bruni, G.P., Lima, K.O. et al. (2017). Cellulose fibers extracted from rice and oat husks and their application in hydrogel. *Food Chemistry* 221: 153–160.
- 21 Kim, G.T., Jeong, S.S., Joost, M. et al. (2011). Use of natural binders and ionic liquid electrolytes for greener and safer lithium-ion batteries. *Journal of Power Sources* 196 (4): 2187–2194.
- 22 Varzi, A., Balducci, A., and Passerini, S. (2014). Natural cellulose: a green alternative binder for high voltage electrochemical double layer capacitors containing ionic liquid-based electrolytes. *Journal of the Electrochemical Society* 161 (3): A368–A375.
- 23 Jeong, S.S., Böckenfeld, N., Balducci, A. et al. (2012). Natural cellulose as binder for lithium battery electrodes. *Journal of Power Sources* 199: 331–335.
- 24 Böckenfeld, N., Jeong, S.S., Winter, M. et al. (2013). Natural, cheap and environmentally friendly binder for supercapacitors. *Journal of Power Sources* 221: 14–20.
- 25 Qiu, X. and Hu, S. (2013). “Smart” materials based on cellulose: a review of the preparations, properties, and applications. *Materials* 6 (3): 738–781.
- 26 Reid, M.L., Brown, M.B., Moss, G.P., and Jones, S.A. (2008). An investigation into solvent-membrane interactions when assessing drug release from organic

- vehicles using regenerated cellulose membranes. *Journal of Pharmacy and Pharmacology* 60 (9): 1139–1147.
- 27 Harini, K. and Sukumar, M. (2019). Development of cellulose-based migratory and nonmigratory active packaging films. *Carbohydrate Polymers* 204 (June 2018): 202–213.
- 28 Dyatkin, B., Presser, V., Heon, M. et al. (2013). Development of a green supercapacitor composed entirely of environmentally friendly materials. *ChemSusChem* 6 (12): 2269–2280.
- 29 Kapu, N.K. and Trajano, H.L. (2014). Review of hemicellulose hydrolysis in softwoods and bamboo. *Biofuels, Bioproducts and Biorefining* 8: 857–870.
- 30 Luo, Y., Li, Z., Li, X. et al. (2019). The production of furfural directly from hemicellulose in lignocellulosic biomass: a review. *Catalysis Today* 319 (December 2017): 14–24.
- 31 Mendes, F.R.S., Bastos, M.S.R., Mendes, L.G. et al. (2017). Preparation and evaluation of hemicellulose films and their blends. *Food Hydrocolloids* 70: 181–190.
- 32 Farhat, W., Venditti, R., Quick, A. et al. (2017). Hemicellulose extraction and characterization for applications in paper coatings and adhesives. *Industrial Crops and Products* 107 (January): 370–377.
- 33 Zhang, J., Wang, Y.H., Qu, Y.S. et al. (2018). Effect of the organizational difference of corn stalk on hemicellulose extraction and enzymatic hydrolysis. *Industrial Crops and Products* 112 (January): 698–704.
- 34 Fernández, M.A., Rissanen, J., Nebreda, A.P. et al. (2018). Hemicelluloses from stone pine, holm oak, and Norway spruce with subcritical water extraction comparative study with characterization and kinetics. *Journal of Supercritical Fluids* 133 (June): 647–657.
- 35 Minjares-Fuentes, R., Femenia, A., Garau, M.C. et al. (2016). Ultrasound-assisted extraction of hemicelluloses from grape pomace using response surface methodology. *Carbohydrate Polymers* 138: 180–191.
- 36 García, J.C., Díaz, M.J., Garcia, M.T. et al. (2013). Search for optimum conditions of wheat straw hemicelluloses cold alkaline extraction process. *Biochemical Engineering Journal* 71: 127–133.
- 37 Ma, X.J., Yang, X.F., Zheng, X. et al. (2014). Degradation and dissolution of hemicelluloses during bamboo hydrothermal pretreatment. *Bioresource Technology* 161: 215–220.
- 38 Liu, X., Luan, S., and Li, W. (2019). Utilization of waste hemicelluloses lye for superabsorbent hydrogel synthesis. *International Journal of Biological Macromolecules* 132: 954–962.
- 39 Zhang, J., Xiao, H., Li, N. et al. (2015). Synthesis and characterization of super-absorbent hydrogels based on hemicellulose. *Journal of Applied Polymer Science* 132 (34): 2–7.
- 40 Salas, Y.A., Colque, M.C., Lazo, A.B. et al. (2008). Obtención y caracterización fisicoquímica y funcional de las fibras dietéticas del níspero común (*Mespilus germanica*). *Revista de la Sociedad Química del Perú* 74 (4): 269–281.

- 41 Naseem, A., Tabasum, S., Zia, K.M. et al. (2016). Lignin-derivatives based polymers, blends and composites: a review. *International Journal of Biological Macromolecules* 93: 296–313.
- 42 Chio, C., Sain, M., and Qin, W. (2019). Lignin utilization: a review of lignin depolymerization from various aspects. *Renewable and Sustainable Energy Reviews* 107 (March): 232–249.
- 43 Ponnusamy, V.K., Nguyen, D.D., Dharmaraja, J. et al. (2019). A review on lignin structure, pretreatments, fermentation reactions and biorefinery potential. *Bioresource Technology* 271 (August 2018): 462–472.
- 44 Doherty, W.O.S., Mousavioun, P., and Fellows, C.M. (2011). Value-adding to cellulosic ethanol: lignin polymers. *Industrial Crops and Products* 33 (2): 259–276.
- 45 Sun, G., Dilcher, D.L., and Zheng, S.L. (2008). A review of recent advances in the study of early angiosperms from northeastern China. *Palaeoworld* 17 (3–4): 166–171.
- 46 Galbe, M. and Zacchi, G. (2002). A review of the production of ethanol from softwood. *Applied Microbiology and Biotechnology* 59 (6): 618–628.
- 47 Wang, X.Q. and Ran, J.H. (2014). Evolution and biogeography of gymnosperms. *Molecular Phylogenetics and Evolution* 75 (1): 24–40.
- 48 Nhuchhen, D., Basu, P., and Acharya, B. (2014). A comprehensive review on biomass torrefaction. *International Journal Renewable Energy and Biofuels* 2014: 1–56.
- 49 Naron, D.R., Collard, F.X., Tyhoda, L., and Görgens, J.F. (2019). Influence of impregnated catalyst on the phenols production from pyrolysis of hardwood, softwood, and herbaceous lignins. *Industrial Crops and Products* 131 (August 2018): 348–356.
- 50 Chakar, F.S. and Ragauskas, A.J. (2004). Review of current and future softwood kraft lignin process chemistry. *Industrial Crops and Products* 20 (2): 131–141.
- 51 Gierer, J. (1980). Chemical aspects of kraft pulping. *Wood Science and Technology* 14 (4): 241–266.
- 52 Gnedenkov, S.V., Sinebryukhov, S.L., Opra, D.P. et al. (2014). Electrochemistry of Klason lignin. *Procedia Chemistry* 11 (96–100): 2014.
- 53 Jung, H.G., Varel, V.H., Weimer, P.J., and Ralph, J. (1999). Accuracy of Klason lignin and acid detergent lignin methods as assessed by bomb calorimetry. *Journal of Agricultural and Food Chemistry* 47: 2005–2008.
- 54 Lora, J. (2010). Industrial commercial lignins: sources, properties and applications. In: *Monomers, Polymers and Composites from Renewable Sources*, Chapter 10, 1e (eds. M.N. Belgacem and A. Gandino), 225–242. Oxford: Elsevier.
- 55 Moreira, P.H.S.S., de Oliveira Freitas, J.C., Braga, R.M. et al. (2018). Production of carboxymethyl lignin from sugar cane bagasse: a cement retarder additive for oilwell application. *Industrial Crops and Products* 116 (August 2017): 144–149.
- 56 Yang, H., Xie, Y., Zheng, X. et al. (2016). Comparative study of lignin characteristics from wheat straw obtained by soda-AQ and kraft pretreatment and effect on the following enzymatic hydrolysis process. *Bioresource Technology* 207: 361–369.

- 57 Mousavioun, P. and Doherty, W.O.S. (2010). Chemical and thermal properties of fractionated bagasse soda lignin. *Industrial Crops and Products* 31 (1): 52–58.
- 58 Chávez, M. and Domine, M. (2013). Lignina, estructura y aplicaciones: métodos de despolimerización para la obtención de derivados aromáticos de interés industrial. lignin, structure and applications: depolymerization methods. *Avances en Ciencia e Ingeniería* 4 (4): 15–46.
- 59 Al Arni, S. (2018). Extraction and isolation methods for lignin separation from sugarcane bagasse: a review. *Industrial Crops and Products* 115 (May 2017): 330–339.
- 60 Schmetz, Q., Maniet, G., Jacquet, N. et al. (2016). Comprehension of an organo-solv process for lignin extraction on *Festuca arundinacea* and monitoring of the cellulose degradation. *Industrial Crops and Products* 94: 308–317.
- 61 Florian, T.D.M., Villani, N., Aguedo, M. et al. (2019). Chemical composition analysis and structural features of banana rachis lignin extracted by two organosolv methods. *Industrial Crops and Products* 132 (September 2018): 269–274.
- 62 Abbasi, T. and Abbasi, S.A. (2010). Biomass energy and the environmental impacts associated with its production and utilization. *Renewable and Sustainable Energy Reviews* 14 (3): 919–937.
- 63 Watkins, D., Nuruddin, M., Hosur, M. et al. (2015). Extraction and characterization of lignin from different biomass resources. *Journal of Materials Research and Technology* 4 (1): 26–32.
- 64 Manara, P., Zabaniotou, A., Vanderghem, C., and Richel, A. (2014). Lignin extraction from Mediterranean agro-wastes: impact of pretreatment conditions on lignin chemical structure and thermal degradation behavior. *Catalysis Today* 223: 25–34.
- 65 Rahimi, A., Ulbrich, A., Coon, J.J., and Stahl, S.S. (2014). Formic-acid-induced depolymerization of oxidized lignin to aromatics. *Nature* 515 (7526): 249–252.
- 66 Guan, G., Kaewpanha, M., Hao, X., and Abudula, A. (2016). Catalytic steam reforming of biomass tar: prospects and challenges. *Renewable and Sustainable Energy Reviews* 58: 450–461.
- 67 Collard, F.X. and Blin, J. (2014). A review on pyrolysis of biomass constituents: mechanisms and composition of the products obtained from the conversion of cellulose, hemicelluloses and lignin. *Renewable and Sustainable Energy Reviews* 38: 594–608.
- 68 Zhang, L., Xu, C., and Champagne, P. (2010). Overview of recent advances in thermo-chemical conversion of biomass. *Energy Conversion and Management* 51 (5): 969–982.
- 69 Biller, P. and Ross, A.B. (2012). Hydrothermal processing of algal biomass for the production of biofuels and chemicals. *Biofuels* 3 (5): 603–623.
- 70 Gollakota, A.R.K., Kishore, N., and Gu, S. (2018). A review on hydrothermal liquefaction of biomass. *Renewable and Sustainable Energy Reviews* 81 (April): 1378–1392.

- 71 Arturi, K.R., Kucheryavskiy, S., Nielsen, R.P. et al. (2019). Molecular footprint of co-solvents in hydrothermal liquefaction (HTL) of *Fallopia Japonica*. *Journal of Supercritical Fluids* 143 (May 2018): 211–222.
- 72 Xu, D., Lin, G., Guo, S. et al. (2018). Catalytic hydrothermal liquefaction of algae and upgrading of biocrude: a critical review. *Renewable and Sustainable Energy Reviews* 97 (August): 103–118.
- 73 Toor, S.S., Rosendahl, L., and Rudolf, A. (2011). Hydrothermal liquefaction of biomass: a review of subcritical water technologies. *Energy* 36 (5): 2328–2342.
- 74 Dermibas, S. (2000). Mechanisms of liquefaction and pyrolysis reactions of biomass. *Energy Conversion and Management* 41: 633–646.
- 75 Titirici, M.M. and Antonietti, M. (2010). Chemistry and materials options of sustainable carbon materials made by hydrothermal carbonization. *Chemical Society Reviews* 39 (1): 103–116.
- 76 Mysyk, R., Gao, Q., Raymundo-Oiñero, E., and Béguin, F. (2012). Microporous carbons finely-tuned by cyclic high-pressure low-temperature oxidation and their use in electrochemical capacitors. *Carbon* 50 (9): 3367–3374.
- 77 Raymundo-Piñero, E., Gao, Q., and Béguin, F. (2013). Carbons for supercapacitors obtained by one-step pressure induced oxidation at low temperature. *Carbon* 61: 278–283.
- 78 Motta, I.L., Miranda, N.T., Filho, R.M., and Maciel, M.R.W. (2018). Biomass gasification in fluidized beds: a review of biomass moisture content and operating pressure effects. *Renewable and Sustainable Energy Reviews* 94: 998–1023.
- 79 Widjaya, E.R., Chen, G., Bowtell, L., and Hills, C. (2018). Gasification of non-woody biomass: a literature review. *Renewable and Sustainable Energy Reviews* 89 (March): 184–193.
- 80 Shahbaz, M., Yusup, S., Inayat, A. et al. (2017). The influence of catalysts in biomass steam gasification and catalytic potential of coal bottom ash in biomass steam gasification: a review. *Renewable and Sustainable Energy Reviews* 73 (November 2015): 468–476.
- 81 Susastriawan, A.A.P., Saptoadi, H., and Purnomo (2017). Small-scale downdraft gasifiers for biomass gasification: a review. *Renewable and Sustainable Energy Reviews* 76 (March): 989–1003.
- 82 Puig-Arnavat, M., Bruno, J.C., and Coronas, A. (2010). Review and analysis of biomass gasification models. *Renewable and Sustainable Energy Reviews* 14 (9): 2841–2851.
- 83 Basu, P. (2010). *Biomass Gasification and Pyrolysis: Practical Design and Theory*, 1e. Burlington: Elsevier Inc.
- 84 Rios, M.L.V., González, A.M., Lora, E.E.S., and del Olmo, O.A.A. (2018). Reduction of tar generated during biomass gasification: a review. *Biomass and Bioenergy* 108 (July 2017): 345–370.
- 85 El-Naggar, A., Lee, S.S., Awad, Y.M. et al. (2018). Influence of soil properties and feedstocks on biochar potential for carbon mineralization and improvement of infertile soils. *Geoderma* 332 (June): 100–108.
- 86 Muñoz, J., Espinosa-Torres, N.D., Guillén-López, A. et al. (2019). Insights into the design of carbon electrodes coming from lignocellulosic components

- pyrolysis with potential application in energy storage devices: a combined in silico and experimental study. *Journal of Analytical and Applied Pyrolysis* 139: 131–144.
- 87 de Velden, M.V., Baeyens, J., Brems, A. et al. (2010). Fundamentals, kinetics and endothermicity of the biomass pyrolysis reaction. *Renewable Energy* 35 (1): 232–242.
- 88 Martínez-Casillas, D.C., Mascorro-Gutiérrez, I., Arreola-Ramos, C.E. et al. (2019). A sustainable approach to produce activated carbons from pecan nut-shell waste for environmentally friendly supercapacitors. *Carbon* 148: 403–412.
- 89 Kleszyk, P., Ratajczak, P., Skowron, P. et al. (2015). Carbons with narrow pore size distribution prepared by simultaneous carbonization and self-activation of tobacco stems and their application to supercapacitors. *Carbon* 81 (1): 148–157.
- 90 Liu, F., Wang, Z., Zhang, H. et al. (2019). Nitrogen, oxygen and sulfur co-doped hierarchical porous carbons toward high-performance supercapacitors by direct pyrolysis of kraft lignin. *Carbon* 149: 105–116.
- 91 Haiping Yang, H., Yan, R., Chin, T. et al. (2004). Thermogravimetric analysis–Fourier transform infrared analysis of palm oil waste pyrolysis. *Energy and Fuels* 18 (6): 1814–1821.
- 92 Chávez-Guerrero, L. and Hinojosa, M. (2010). Bagasse from the mezcal industry as an alternative renewable energy produced in arid lands. *Fuel* 89 (12): 4049–4052.
- 93 Qian, J.M., Wang, J.P., Qiao, G.J., and Jin, Z.H. (2004). Preparation of porous SiC ceramic with a woodlike microstructure by sol–gel and carbothermal reduction processing. *Journal of the European Ceramic Society* 24 (10–11): 3251–3259.
- 94 Mohan, D., Pittman, C.U., and Steele, P.H. (2006). Pyrolysis of wood/biomass for bio-oil: a critical review. *Energy and Fuels* 20 (4): 848–889.
- 95 Cagnon, B., Py, X., Guilloit, A. et al. (2009). Contributions of hemicellulose, cellulose and lignin to the mass and the porous properties of chars and steam activated carbons from various lignocellulosic precursors. *Bioresource Technology* 100 (1): 292–298.
- 96 Haiping Yang, H., Yan, R., Chen, H. et al. (2006). In-depth investigation of biomass pyrolysis based on three major components: hemicellulose, cellulose and lignin. *Energy and Fuels* 20 (1): 388–393.
- 97 Stefanidis, S.D., Kalogiannis, K.G., Iliopoulou, E.F. et al. (2014). A study of lignocellulosic biomass pyrolysis via the pyrolysis of cellulose, hemicellulose and lignin. *Journal of Analytical and Applied Pyrolysis* 105: 143–150.
- 98 Haiping Yang, H., Yan, R., Chen, H. et al. (2007). Characteristics of hemicellulose, cellulose and lignin pyrolysis. *Fuel* 86 (12–13): 1781–1788.
- 99 Henrich, E., Dahmen, N., Weirich, F. et al. (2016). Fast pyrolysis of lignocellulosics in a twin screw mixer reactor. *Fuel Processing Technology* 143: 151–161.
- 100 Russell, S.H., Turrion-Gomez, J.J., Meredith, W. et al. (2017). Increased charcoal yield and production of lighter oils from the slow pyrolysis of biomass. *Journal of Analytical and Applied Pyrolysis* 124: 536–541.
- 101 Bridgwater, A.V. (2012). Review of fast pyrolysis of biomass and product upgrading. *Biomass and Bioenergy* 38: 68–94.

- 102 Quispe, I., Navia, R., and Kahhat, R. (2017). Energy potential from rice husk through direct combustion and fast pyrolysis: a review. *Waste Management* 59: 200–210.
- 103 Park, H.J., Dong, J.I., Jeon, J.K. et al. (2008). Effects of the operating parameters on the production of bio-oil in the fast pyrolysis of Japanese larch. *Chemical Engineering Journal* 143 (1–3): 124–132.
- 104 Kebelmann, K., Hornung, A., Karsten, U., and Griffiths, G. (2013). Intermediate pyrolysis and product identification by TGA and Py-GC/MS of green microalgae and their extracted protein and lipid components. *Biomass and Bioenergy* 49: 38–48.
- 105 Mohammed, I.Y., Kazi, F.K., Yusup, S. et al. (2016). Catalytic intermediate pyrolysis of Napier grass in a fixed bed reactor with ZSM-5, HZSM-5 and zinc-exchanged zeolite-a as the catalyst. *Energies* 9 (4): 246–263.
- 106 Park, J., Lee, Y., Ryu, C., and Park, Y.K. (2014). Slow pyrolysis of rice straw: analysis of products properties, carbon and energy yields. *Bioresource Technology* 155: 63–70.
- 107 Klug, M., Gamboa, N., and Lorber, K. (2013). Sustainable development and renewable energy from biomass in Peru – overview of the current situation and research with a bench scale pyrolysis reactor to use organic waste for energy production. *Journal of Sustainable Development* 6 (8): 130–139.
- 108 Roberts, D.A., Cole, A.J., Whelan, A. et al. (2017). Slow pyrolysis enhances the recovery and reuse of phosphorus and reduces metal leaching from biosolids. *Waste Management* 64: 133–139.
- 109 Zeng, K., Flamant, G., Gauthier, D., and Guillot, E. (2015). Solar pyrolysis of wood in a lab-scale solar reactor: influence of temperature and sweep gas flow rate on products distribution. *Energy Procedia* 69: 1849–1858.
- 110 Andrade, L.A., Barrozo, M.A.S., and Vieira, L.G.M. (2018). Catalytic solar pyrolysis of microalgae *Chlamydomonas reinhardtii*. *Solar Energy* 173 (August): 928–938.
- 111 Nzihou, A., Flamant, G., and Stanmore, B. (2012). Synthetic fuels from biomass using concentrated solar energy – a review. *Energy* 42 (1): 121–131.
- 112 Ayala-Cortés, A., Lobato-Peralta, D.R., Arreola-Ramos, C.E. et al. (2019). Exploring the influence of solar pyrolysis operation parameters on characteristics of carbon materials. *Journal of Analytical and Applied Pyrolysis* 140: 290–298.
- 113 Kambo, H.S. and Dutta, A. (2015). A comparative review of biochar and hydrochar in terms of production, physico-chemical properties and applications. *Renewable and Sustainable Energy Reviews* 45: 359–378.
- 114 Tan, Z., Lin, C.S.K., Ji, X., and Rainey, T.J. (2017). Returning biochar to fields: a review. *Applied Soil Ecology* 116 (March): 1–11.
- 115 Sing, K. (2001). The use of nitrogen adsorption for the characterization of porous materials. *Colloids and Surfaces A: Physicochemical and Engineering Aspects* 187–188: 3–9.
- 116 Li, H., Dong, X., da Silva, E.B. et al. (2017). Mechanisms of metal sorption by biochars: biochar characteristics and modifications. *Chemosphere* 178: 466–478.

- 117** Shaaban, M., Zwietyen, L.V., Bashir, S. et al. (2018). A concise review of biochar application to agricultural soils to improve soil conditions and fight pollution. *Journal of Environmental Management* 228 (August): 429–440.
- 118** Cuentas-Gallegos, A.K., Pacheco-Catalán, D., and Miranda-Hernández, M. (2016). Environmentally friendly supercapacitors. In: *Materials for Sustainable Energy Applications*, 1e, vol. 3, Chapter 8 (eds. X. Moya and D. Muñoz-Rojas), 345–486. Pan Stanford Publishing Pvt. Ltd.
- 119** Jain, A. and Tripathi, S.K. (2014). Fabrication and characterization of energy storing supercapacitor devices using coconut shell based activated charcoal electrode. *Materials Science and Engineering B: Solid-State Materials for Advanced Technology* 183 (1): 54–60.
- 120** González-García, P. (2018). Activated carbon from lignocellulosics precursors: a review of the synthesis methods, characterization techniques and applications. *Renewable and Sustainable Energy Reviews* 82 (August 2017): 1393–1414.
- 121** Sandoval, J.M., Espinoza Trujillo, M.J., Flota Bunuelos, M.I., Duran Gomez, J.L., Verde Gomez, J.Y., and Pacheco-Catalan, D.E. (2013). Batteries-supercapacitors storage systems for a mobile hybrid renewable energy system. 2013 IEEE Electrical Power and Energy Conference, EPEC, 01(280955) (21–23 August 2013), Halifax, NS, Canada.
- 122** Poonam, S.K., Arora, A., and Tripathi, S.K. (2019). Review of supercapacitors: materials and devices. *Journal of Energy Storage* 21: 801–825.
- 123** Wang, C., Xiong, Y., Wang, H., and Sun, Q. (2018). All-round utilization of biomass derived all-solid-state asymmetric carbon-based supercapacitor. *Journal of Colloid and Interface Science* 528: 349–359.
- 124** Becker, H.I. (1957). US Patent No. 2800616.
- 125** Muzaffar, A., Ahamed, M.B., Deshmukh, K., and Thirumalai, J. (2019). A review on recent advances in hybrid supercapacitors: design, fabrication and applications. *Renewable and Sustainable Energy Reviews* 101 (October 2018): 123–145.
- 126** Zhang, Y., Feng, H., Wu, X. et al. (2009). Progress of electrochemical capacitor electrode materials: a review. *International Journal of Hydrogen Energy* 34 (11): 4889–4899.
- 127** Faraji, S. and Ani, F.N. (2014). Microwave-assisted synthesis of metal oxide/hydroxide composite electrodes for high power supercapacitors – a review. *Journal of Power Sources* 263: 338–360.
- 128** Von Helmholtz, H. (1853). Ueber einige Gesetze der Vertheilung elektrischer Ströme in körperlichen Leitern mit Anwendung auf die thierisch-elektrischen Versuche. *Annalen der Physik und Chemie* 7: 211–233.
- 129** González, A., Goikolea, E., Barrena, J.A., and Mysyk, R. (2016). Review on supercapacitors: technologies and materials. *Renewable and Sustainable Energy Reviews* 58: 1189–1206.
- 130** Endo, M., Takeda, T., Kim, Y.J. et al. (2014). High power electric double layer capacitor (EDLC's); from operating principles to pore size control in advanced activated carbons. *Carbon Science* 2001. *Carbon Science* 1 (January 2001): 117–128.

- 131 Simon, P. and Gogotsi, Y. (2008). Materials for electrochemical capacitors. *Nature Materials* 7 (11): 845–854.
- 132 Gouy, L.G. (1910). Sur la constitution de la charge électrique à la surface d'un électrolyte. *Journal de Physique Théorique et Appliquée* 9 (1): 457–468.
- 133 Chapman, D.L. (1913). A contribution to the theory of electrocapillarity. *The London, Edinburgh, and Dublin Philosophical Magazine and Journal of Science* 25 (148): 475–481.
- 134 Stern, O. (1924). Zur theorie der elektrolytischen doppelschicht. *Zeitschrift für Elektrochemie und Angewandte Physikalische Chemie* 30: 508–516.
- 135 Huang, C., Sun, T., and Hulicova-Jurcakova, D. (2013). Wide electrochemical window of supercapacitors from coffee bean-derived phosphorus-rich carbons. *ChemSusChem* 6 (12): 2330–2339.
- 136 Qiu, Z., Wang, Y., Bi, X. et al. (2018). Biochar-based carbons with hierarchical micro-meso-macro porosity for high rate and long cycle life supercapacitors. *Journal of Power Sources* 376 (August 2017): 82–90.
- 137 Pourhosseini, S.E.M., Norouzi, O., and Naderi, H.R. (2017). Study of micro/macro ordered porous carbon with olive-shaped structure derived from *Cladophora glomerata* macroalgae as efficient working electrodes of supercapacitors. *Biomass and Bioenergy* 107 (May): 287–298.
- 138 Wang, J.R., Wan, F., Lü, Q.-F. et al. (2018). Self-nitrogen-doped porous biochar derived from kapok (*Ceiba insignis*) fibers: effect of pyrolysis temperature and high electrochemical performance. *Journal of Materials Science and Technology* 34 (10): 1959–1968.
- 139 Zou, R., Quan, H., Wang, W. et al. (2018). Porous carbon with interpenetrating framework from *Osmanthus* flower as electrode materials for high-performance supercapacitor. *Journal of Environmental Chemical Engineering* 6 (1): 258–265.
- 140 Qu, S., Wan, J., Dai, C. et al. (2018). Promising as high-performance supercapacitor electrode materials porous carbons derived from biological lotus leaf. *Journal of Alloys and Compounds* 751: 107–116.
- 141 Fic, K., Platek, A., Piwek, J., and Frackowiak, E. (2018). Sustainable materials for electrochemical capacitors. *Materials Today* 21 (4): 437–454.
- 142 Saha, D., Li, Y., Bi, Z. et al. (2014). Studies on supercapacitor electrode material from activated lignin-derived mesoporous carbon. *Langmuir* 30 (3): 900–910.
- 143 Nieto-Delgado, C. and Rangel-Mendez, J.R. (2013). In situ transformation of agave bagasse into activated carbon by use of an environmental scanning electron microscope. *Microporous and Mesoporous Materials* 167: 249–253.
- 144 Ioannidou, O. and Zabaniotou, A. (2007). Agricultural residues as precursors for activated carbon production – a review. *Renewable and Sustainable Energy Reviews* 11 (9): 1966–2005.
- 145 Kilpimaa, S., Runtti, H., Kangas, T. et al. (2015). Physical activation of carbon residue from biomass gasification: novel sorbent for the removal of phosphates and nitrates from aqueous solution. *Journal of Industrial and Engineering Chemistry* 21: 1354–1364.
- 146 Do, D.D. and Words-coal, K. (1996). The preparation of active carbons from coal by chemical and physical activation. *Carbon* 34 (4): 471–479.

- 147 Martínez-Casillas, D.C., Alonso-Lemus, I.L., Mascorro-Gutiérrez, I., and Cuentas-Gallegos, A.K. (2018). Leather waste-derived biochar with high performance for supercapacitors. *Journal of the Electrochemical Society* 165 (10): A2061–A2068.
- 148 Bouchelta, C., Medjram, M.S., Bertrand, O., and Bellat, J.P. (2008). Preparation and characterization of activated carbon from date stones by physical activation with steam. *Journal of Analytical and Applied Pyrolysis* 82 (1): 70–77.
- 149 Marsh, H. and Rodríguez-Reinoso, F. (2007). Chapter 5: Activation process (thermal or physical). In: *Activated Carbon*. Elsevier. ISBN: 9780080455969.
- 150 El-Hendawy, A.N.A., Alexander, A.J., Andrews, R.J., and Forrest, G. (2008). Effects of activation schemes on porous, surface and thermal properties of activated carbons prepared from cotton stalks. *Journal of Analytical and Applied Pyrolysis* 82 (2): 272–278.
- 151 Li, Z.Y., Akhtar, M.S., Kwak, D.H., and Yang, O.B. (2017). Improvement in the surface properties of activated carbon via steam pretreatment for high performance supercapacitors. *Applied Surface Science* 404: 88–93.
- 152 Jiménez-Cordero, D., Heras, F., Gilarranz, M.A., and Raymundo-Piñero, E. (2014). Grape seed carbons for studying the influence of texture on supercapacitor behaviour in aqueous electrolytes. *Carbon* 71: 127–138.
- 153 Dizbay-Onat, M., Vaidya, U.K., and Lungu, C.T. (2017). Preparation of industrial sisal fiber waste derived activated carbon by chemical activation and effects of carbonization parameters on surface characteristics. *Industrial Crops and Products* 95: 583–590.
- 154 Nieto-Delgado, C., Terrones, M., and Rangel-Mendez, J.R. (2011). Development of highly microporous activated carbon from the alcoholic beverage industry organic by-products. *Biomass and Bioenergy* 35 (1): 103–112.
- 155 Xi, Y., Wang, Y., Yang, D. et al. (2019). K_2CO_3 activation enhancing the graphitization of porous lignin carbon derived from enzymatic hydrolysis lignin for high performance lithium-ion storage. *Journal of Alloys and Compounds* 785: 706–714.
- 156 Yue, L., Xia, Q., Wang, L. et al. (2018). CO_2 adsorption at nitrogen-doped carbons prepared by K_2CO_3 activation of urea-modified coconut shell. *Journal of Colloid and Interface Science* 511: 259–267.
- 157 Valizadeh, S., Younesi, H., and Bahramifar, N. (2016). Highly mesoporous K_2CO_3 and KOH/activated carbon for SDBS removal from water samples: batch and fixed-bed column adsorption process. *Environmental Nanotechnology, Monitoring and Management* 6: 1–13.
- 158 Wei, Q., Chen, Z., Cheng, Y. et al. (2019). Preparation and electrochemical performance of orange peel based-activated carbons activated by different activators. *Colloids and Surfaces A: Physicochemical and Engineering Aspects* 574 (January): 221–227.
- 159 Hsu, L.Y. and Teng, H. (2000). Influence of different chemical reagents on the preparation of activated carbons from bituminous coal. *Fuel Processing Technology* 64 (1): 155–166.

- 160** Deng, H., Li, G., Yang, H. et al. (2010). Preparation of activated carbons from cotton stalk by microwave assisted KOH and K_2CO_3 activation. *Chemical Engineering Journal* 163 (3): 373–381.
- 161** Miller, E.E., Hua, Y., and Tezel, F.H. (2018). Materials for energy storage: review of electrode materials and methods of increasing capacitance for supercapacitors. *Journal of Energy Storage* 20 (August): 30–40.
- 162** Brousse, T., Bélanger, D., and Long, J.W. (2015). To be or not to be pseudocapacitive? *Journal of the Electrochemical Society* 162 (5): A5185–A5189.
- 163** Conway, B.E. and Pell, W.G. (2003). Double-layer and pseudocapacitance types of electrochemical capacitors and their applications to the development of hybrid devices. *Journal of Solid State Electrochemistry* 7 (9): 637–644.
- 164** Lee, S.H. and Im, I.H. (2018). Excellent performance hybrid supercapacitors based on $LiNi_{1/3}Mn_{1/3}Co_{1/3}O_2$ /activated carbon electrode. *Materials Letters* 231: 38–42.
- 165** Liu, L., Chen, T., Rong, H., and Wang, Z. (2018). $NiCo_2S_4$ nanosheets network supported on Ni foam as an electrode for hybrid supercapacitors. *Journal of Alloys and Compounds* 766: 149–156.
- 166** Hu, X., Nan, H., Liu, M. et al. (2019). Battery-like $MnCo_2O_4$ electrode materials combined with active carbon for hybrid supercapacitors. *Electrochimica Acta* 306: 599–609.
- 167** Zhang, Z., Du, W., Ren, X. et al. (2019). $Ni(OH)_2-Co_2(OH)_3Cl$ bilayer nanocomposites supported by Ni foams for binder-free electrodes of high-performance hybrid supercapacitors. *Applied Surface Science* 469 (July 2018): 624–633.
- 168** Rafai, S., Qiao, C., Naveed, M. et al. (2019). Microwave-anion-exchange route to ultrathin cobalt-nickel-sulfide nanosheets for hybrid supercapacitors. *Chemical Engineering Journal* 362 (December 2018): 576–587.
- 169** Kannangara, Y.Y., Rathnayake, U.A., and Song, J.K. (2019). Hybrid supercapacitors based on metal organic frameworks using *p*-phenylenediamine building block. *Chemical Engineering Journal* 361 (December 2018): 1235–1244.
- 170** Kim, H.K. and Lee, S.H. (2016). Enhanced electrochemical performances of cylindrical hybrid supercapacitors using activated carbon/ $Li_{4-x}M_xTi_{5-y}N_yO_{12}$ ($M = Na, N = V, Mn$) electrodes. *Energy* 109: 506–511.
- 171** Qin, W., Wu, L., Zheng, Z. et al. (2014). Lignin hydrolysis and phosphorylation mechanism during phosphoric acid-acetone pretreatment: a DFT study. *Molecules* 19: 21335–21349.
- 172** Chenoweth, K., van Duin, A.C.T., and Goddard, W.A. (2008). ReaxFF reactive force field for molecular dynamics simulations of hydrocarbon oxidation. *The Journal of Physical Chemistry A* 112: 1040–1053.
- 173** Delley, B. (1990). An allelectron numerical method for solving the local density functional for polyatomic molecules. *The Journal of Chemical Physics* 92: 508–517.
- 174** Peng, C. and Schlegel, H.B. (1993). Combining synchronous transit and quasi-newton methods to find transition states. *Israel Journal of Chemistry* 33: 449–454.

- 175 Sangha, A.K., Petridis, L., Smith, J.C. et al. (2012). Molecular simulation as a tool for studying lignin. *Environmental Progress & Sustainable Energy* 31 (1): 47–54.
- 176 Karhunen, P., Rummakko, P., Sipila, J. et al. (1995). Dibenzodioxocins; a novel type of linkage in softwood lignins. *Tetrahedron Letters* 36: 169–170.
- 177 Karhunen, P., Rummakko, P., Sipila, J. et al. (1995). The formation of dibenzodioxocin structures by oxidative coupling. A model reaction for lignin biosynthesis. *Tetrahedron Letters* 36: 4501–4504.
- 178 Jiang, X., Lu, Q., Hu, B. et al. (2018). Intermolecular interaction mechanism of lignin pyrolysis: a joint theoretical and experimental study. *Fuel* 215: 386–394.
- 179 Frisch, M.J., Trucks, G.W., Schlegel, H.B. et al. (2009). *Gaussian, 09:E.01*. Gaussian.
- 180 Cramer, C.J. (2005). *Essentials of Computational Chemistry: Theories and Models*. Wiley.
- 181 Stewart, J.J.P. (1989). Optimization of parameters for semiempirical methods I. Method. *Journal of Computational Chemistry* 10: 209–220.
- 182 Dewar, M.J.S., Zoebisch, E.G., Healy, E.F., and Stewart, J.J.P. (1985). Development and use of quantum mechanical molecular models. 76. AM1: a new general purpose quantum mechanical molecular model. *Journal of the American Chemical Society* 107: 3902–3909.
- 183 Repasky, M.P., Chandrasekhar, J., and Jorgensen, W.L. (2002). PDDG/PM3 and PDDG/MNDO: improved semiempirical methods. *Journal of Computational Chemistry* 23: 1601–1622.
- 184 Beste, A. and Buchanan, A.C. (2009). Computational study of bond dissociation enthalpies for lignin model compounds. Substituent effects in phenethyl phenyl ethers. *The Journal of Organic Chemistry* 74: 2837–2841.
- 185 Beste, A. and Buchanan, A.C. (2010). Substituent effects on the reaction rates of hydrogen abstraction in the pyrolysis of phenethyl phenyl ethers. *Energy & Fuels* 24: 2857–2867.
- 186 Durbeej, B. and Eriksson, L.A. (2003). Spin distribution in dehydrogenated coniferyl alcohol and associated dilignol radicals. *Holzforschung* 57: 59–61.
- 187 Durbeej, B. and Eriksson, L. (2003). A density functional theory study of coniferyl alcohol intermonomeric cross linkages in lignin – three-dimensional structures, stabilities and the thermodynamic control hypothesis. *Holzforschung* 57 (2): 150–164.
- 188 Durbeej, B. and Eriksson, L. (2003). Formation of β -O-4 lignin models: a theoretical study. *Holzforschung* 57 (2): 466–478.
- 189 Becke, A.D. (1993). Density functional thermochemistry. III. The role of exact exchange. *The Journal of Chemical Physics* 98 (7): 5648–5652.
- 190 Huang, J. and He, C. (2015). Pyrolysis mechanism of α -O-4 linkage lignin dimer: a theoretical study. *Journal of Analytical and Applied Pyrolysis* 113: 655–664.
- 191 Beste, A., Buchanan, A.C., Britt, P.F. et al. (2007). Kinetic analysis of the pyrolysis of phenethyl phenyl ether: computational prediction of α/β -selectivities. *The Journal of Physical Chemistry A* 111 (48): 12118–12126.

- 192 Beste, A., Buchanan, A.C., and Harrison, R.J. (2008). Computational prediction of α/β selectivities in the pyrolysis of oxygen-substituted phenethyl phenyl ethers. *The Journal of Physical Chemistry A* 112: 4982–4988.
- 193 Besombes, S. and Mazeau, K. (2004). Molecular dynamics simulations of a guaiacyl β -O-4 lignin model compound: examination of intramolecular hydrogen bonding and conformational flexibility. *Biopolymers* 73: 301–315.
- 194 Besombes, S., Utille, J.P., Mazeau, K. et al. (2004). Conformational study of a guaiacyl β -O-4 lignin model compound by NMR. Examination of intra-molecular hydrogen bonding interactions and conformational flexibility in solution. *Magnetic Resonance in Chemistry* 42: 337–347.
- 195 Besombes, S. and Mazeau, K. (2005). The cellulose/lignin assembly assessed by molecular modeling. Part 1: adsorption of a three guaiacyl β -O-4 dimer onto a I β cellulose whisker. *Plant Physiology and Biochemistry* 43: 299–308.
- 196 Besombes, S. and Mazeau, K. (2005). The cellulose/lignin assembly assessed by molecular modeling. Part 2: seeking for evidence of organization of lignin molecules at the interface with cellulose. *Plant Physiology and Biochemistry* 43: 277–286.
- 197 Petridis, L. and Smith, J.C. (2009). A molecular mechanics force field for lignin. *Journal of Computational Chemistry* 30: 457–467.
- 198 MacKerell, A.D., Bashford, D., Bellott, M. et al. (1998). All-atom empirical potential for molecular modeling and dynamics studies of proteins. *The Journal of Physical Chemistry B* 102: 3586–3616.
- 199 Petridis, L., Pingali, S.V., Urban, V. et al. (2011). Self-similar multi-scale structure of lignin revealed by neutron scattering and molecular dynamics simulation. *Physical Review E* 83: 061911.
- 200 Schulz, R., Lindner, B., Petridis, L., and Smith, J.C. (2009). Scaling of multimillion-atom biological molecular dynamics simulation on a petascale supercomputer. *Journal of Chemical Theory and Computation* 5 (10): 2798–2808.
- 201 Matthews, J.F., Skopec, C.E., Mason, P.E. et al. (2006). Computer simulation studies of microcrystalline cellulose I β . *Carbohydrate Research* 341: 138–152.
- 202 Youssefian, S. and Rahbar, N. (2015). Molecular origin of strength and stiffness in bamboo fibrils. *Scientific Reports* 5: 11116.
- 203 Sun, H., Ren, P., and Fried, J.R. (1998). The COMPASS force field: parameterization and validation for phosphazenes. *Computational and Theoretical Polymer Science* 8: 229–246.
- 204 Bazooyar, F., Momany, F.A., and Bolton, K. (2012). Validating empirical force fields for molecular-level simulation of cellulose dissolution. *Computational and Theoretical Chemistry* 984: 119–127.
- 205 Janesko, B.G. (2001). Modeling interactions between lignocellulose and ionic liquids using DFT-D. *Physical Chemistry Chemical Physics* 13: 11393–11401.
- 206 Grimme, S. (2006). Semiempirical GGA-type density functional constructed with a long-range dispersion correction. *Journal of Computational Chemistry* 27: 1787–1799.
- 207 Cancès, E., Mennucci, B., and Tomasi, J. (1997). A new integral equation formalism for the polarizable continuum model: theoretical background and

- applications to isotropic and anisotropic dielectrics. *The Journal of Chemical Physics* 107: 3032–3041.
- 208 Stewart, J.J.P. (2007). Optimization of parameters for semiempirical methods V: modification of NDDO approximations and application to 70 elements. *Journal of Molecular Modeling* 13: 1173–1213.
- 209 Zhang, T., Li, X., and Guo, L. (2017). Initial reactivity of linkages and monomer rings in lignin pyrolysis revealed by ReaxFF molecular dynamics. *Langmuir* 33: 11646–11657.
- 210 van Duin, A.C.T., Dasgupta, S., Lorant, F., and Goddard, W.A. III, (2001). ReaxFF: a reactive force field for hydrocarbons. *The Journal of Physical Chemistry* 105: 9396–9409.
- 211 Adler, E. (1977). Lignin chemistry – past, present and future. *Wood Science and Technology* 11 (3): 169–218.
- 212 Zheng, M., Li, X., and Guo, L. (2013). Algorithms of GPU-enabled reactive force field (ReaxFF) molecular dynamics. *Journal of Molecular Graphics and Modelling* 41: 1–11.
- 213 Plimpton, S. (1995). Fast parallel algorithms for short-range molecular dynamics. *Journal of Computational Physics* 117 (1): 1–19.
- 214 Pan, T. and Cheng, C. (2015). An ab initio molecular dynamics analysis of lignin as a potential antioxidant for hydrocarbons. *Journal of Molecular Graphics and Modelling* 62: 325–341.
- 215 Qi, T., Bauschlicher, C.W., Lawson, J.W. et al. (2013). Comparison of ReaxFF, DFTB, and DFT for phenolic pyrolysis. 1. Molecular dynamics simulations. *The Journal of Physical Chemistry A* 117: 11115–11125.
- 216 Elstner, M., Porezag, D., Jungnickel, G. et al. (1998). Self-consistent-charge density-functional tight-binding method for simulations of complex materials properties. *Physical Review B* 58: 7260–7268.
- 217 Aradi, B., Hourahine, B., and Frauenheim, T. (2007). DFTB+, a sparse matrix-based implementation of the DFTB method. *The Journal of Physical Chemistry A* 111 (5678–5684): 2007.
- 218 Kresse, G. and Joubert, D. (1999). From ultrasoft pseudopotentials to the projector augmented-wave method. *Physical Review B* 59: 1758–1775.
- 219 Kresse, G. and Furthmüller, J. (1996). Efficient iterative schemes for ab initio total-energy calculations using a plane-wave basis set. *Physical Review B* 54: 11169–11186.
- 220 Zhang, T., Li, X., Qiao, X. et al. (2016). Initial mechanisms for an overall behavior of lignin pyrolysis through large-scale ReaxFF molecular dynamics simulations. *Energy & Fuels* 30: 3140–3150.
- 221 Mar, B.D. and Kulik, H.J. (2017). Depolymerization pathways for branching lignin spirodienone units revealed with ab initio steered molecular dynamics. *The Journal of Physical Chemistry A* 121: 532–543.
- 222 Ufimtsev, S.I. and Martinez, T.J. (2009). Quantum chemistry on graphical processing units. 3. Analytical energy gradients, geometry optimization, and first principles molecular dynamics. *Journal of Chemical Theory and Computation* 5: 2619–2628.

- 223** Henkelman, G., Uberuaga, B.P., and Jónsson, H. (2000). A climbing image nudged elastic band method for finding saddle points and minimum energy paths. *The Journal of Chemical Physics* 113: 9901–9904.
- 224** Muñiz, J., Espinosa-Torres, N.D., Guillén-López, A. et al. (2019). Geometrical structure data of nanoporous carbon systems obtained from computer simulated pyrolysis. *Data in Brief* 24: 103874.
- 225** Pandolfo, A.G. and Hollenkamp, A.F. (2006). Carbon properties and their role in supercapacitors. *Journal of Power Sources* 157: 11–27.
- 226** van Duin, A.C.T., Strachan, A., Stewman, S. et al. (2003). ReaxFF_{SiO} reactive force field for silicon and silicon oxide systems. *The Journal of Physical Chemistry A* 107: 3803–3811.
- 227** Bo, Z., Li, C., Yang, H. et al. (2018). Design of supercapacitor electrodes using molecular dynamics simulations. *Nano-Micro Letters* 10 (2): 33.
- 228** Rajput, N.N., Monk, J., and Hung, F.R. (2014). Ionic liquids confined in a realistic activated carbon model: a molecular simulation study. *The Journal of Physical Chemistry C* 118 (3): 1540–1553.
- 229** McGreevy, R.L. and Pusztai, L. (1988). Reverse Monte Carlo simulation: a new technique for the determination of disordered structures. *Molecular Simulation* 1 (6): 359–367.
- 230** Fei Zhang, F., Yu, Z., Rondinone, A.J. et al. (2018). Adsorption of molecular nitrogen in electrical double layers near planar and atomically sharp electrodes. *Langmuir* 34 (48): 14552–14561, PMID: 30411900.
- 231** McNutt, N.W., Rios, O., Maroulas, V., and Keffer, D.J. (2017). Interfacial Li-ion localization in hierarchical carbon anodes. *Carbon* 111: 828–834.

